DEC 16 1997

SANDIA REPORT

SAND97–2765 • UC–705
Unlimited Release
Printed November 1997

Simulation of Armor Penetration by Tungsten Rods: ALEGRA Validation Report

RECEIVED
DEC 2 2 1997
OSTI

Daniel E. Carroll, Eugene S. Hertel, Jr., Timothy G. Trucano

MASTER

Prepared by
Sandia National Laboratories
Albuquerque, New Mexico 87185 and Livermore, California 94550

Sandia is a multiprogram laboratory operated by Sandia Corporation,
a Lockheed Martin Company, for the United States Department of
Energy under Contract DE-AC04-94AL85000.

DISTRIBUTION OF THIS DOCUMENT IS UNLIMITED

Approved for public release; further dissemination unlimited.

Sandia National Laboratories

Simulation of Armor Penetration by Tungsten Rods: ALEGRA Validation Report

Daniel E. Carroll
Eugene S. Hertel, Jr.
Timothy G. Trucano
Computational Physics Research and Development Department
Sandia National Laboratories
P.O. Box 5800
Albuquerque, NM 87185-0819

Abstract

Results from simulations of the impact and penetration of tungsten alloy rods into thick rolled armor plates are presented. The calculations were performed with the CTH and ALEGRA computer codes using the DOE massively parallel TFLOPS computer co-developed by Sandia National Laboratory and Intel Corporation. Comparisons with experimental results are presented. Agreement of the two codes with each other and with the empirical results for penetration channel depth and radius is very close. Other shock physics and penetration features are also compared to simulation results.

Contents

List of Figures

List of Tables

Executive Summary

The penetration of long rods into thick targets is a significant simulation challenge. Successfully matching experimental residual cavity data requires accurate Eulerian hydrodynamics for both material movement and shock wave propagation, as well as accurate material equation of state (EOS) and strength models. Such calculations are sensitive to meshing resolution and typically require significant hardware capability to perform mesh converged calculations.

This report presents the results of simulations performed using the CTH and ALEGRA shock physics codes to model the penetration of "long" tungsten alloy rods into thick (semi-infinite) rolled armor plates. The experiments are well documented and results are available in both a published paper [3] and an unpublished data report [4]. Computational meshes were used that resolved the physics and have been shown to be of sufficient resolution in previous work of this nature [10]. The mesh used was essentially identical for the two codes and the options were chosen to keep the operation of the two codes very similar. A detailed description of the mesh used and the code options that were chosen is presented.

Results for the simulations for penetration channel and depth are compared to experimental results in Figures 6 and 7. Simulation results for channel depth, with a single exception for CTH, were all within 10% of experimental results and often within 5%. Channel radius computations were within 20% of experimental values and tended to be too large. While the percentage error in radius is larger than that for the depth results, the uncertainties in these values are much larger since they are closer to the experimental and numerical error values. Wave propagation features in the tungsten rod and penetration velocities are also compared with analytical models. Close agreement is observed and discussed. In particular, analytic modeling is in good agreement with these calculations for the speed of penetration of typical rods.

The calculations were performed on the DOE Teraflop computer, co-developed by Sandia and Intel Corporation, as well as SUN and Hewlett-Packard scientific workstations.

Because the present calculations were performed in 2-D axisymmetric geometry, this study does not constitute a validation study for 3-D ALEGRA hydrodynamics modules. It also is the case that material fracture is not particularly important in these types of impacts (since we are not examining penetrations close to the ballistic limit of the target). A stearner validation test similar to this study would be to match in-flight dynamic radiography of the penetrator. This type of data is not readily available.

Finally, more general mesh hydrodynamics - a combination of single material ALE (Arbitrary-Lagrangian Eulerian) and multi-material ALE - was not attempted for these calculations. Such a study will be the content of a future report. We also have not studied in this report the use of Lagrangian subcycling in Eulerian calculations using ALEGRA.

We have compared ALEGRA calculations with CTH calculations in this study. The purpose of this was to test code specific issues of similarity (or not) in the numerical

hydrodynamics, as well as in the material models. Differences between CTH and ALEGRA in this study are assumed to be due to known differences between the two codes in the following specifics:

- Finite-difference versus finite element formulations.
- Face-centered versus node centered velocity fields.
- Different treatments of the stress tensor.
- Different treatment of stress in multi-material cells.

In all matters of validated accuracy, the only comparison of importance was between ALEGRA and the presented data. This report should be considered with this viewpoint in mind.

Intentionally Left Blank

Simulation of Armor Penetration by Tungsten Rods

Introduction

This work arises from a desire to have a documented comparison of computational ALEGRA code results with experimental results in penetration-type problems. A secondary reason for the work is to document a comparison between results produced by the CTH and ALEGRA codes.

The experimental results will first be briefly described, with an explanation of the rationale employed to choose particular experiments to model. Next, the two computer codes will be briefly described. The problem setups are then described along with models used and parameters employed therein. Calculations performed on a network of workstations and on the DOE Teraflop massively parallel computer, co-developed by Sandia National Laboratory and Intel Corp., are described and the results of the calculations are presented. These results are then discussed and directions for future work are outlined.

Experimental Results

The calculational results reported in this work simulate a series of experiments that were performed by Silsby and reported in 1984 [3]. The experiments employed both a conventional powder gun at Range 12 (R12), Terminal Ballistics Division, Ballistic Research Laboratory and the von Karman Facility's G (VKG) Range two-stage light gas gun to fire long tungsten alloy rods into semi-infinite slabs of rolled homogeneous armor (RHA). The rods are described as long because their length-to-diameter ratio (L/D) is large, ~23. Two types of rods, with mass of approximately 50 and 100 grams, were fired at velocities ranging from 1300 to 4500 m/s. A report describing the results obtained at VKG contains details of most of the experiments and the full test matrix [4].

For calculational comparisons, six of the fourteen tests were selected. These tests, 1929, 5835, 5839, 5841, 5842 and 5844 represent the smallest values of yaw in the series that are still consistent with a wide range of impact velocities. Three of the tests, 5841, 5842 and 5844, used "50" g rods, while the balance used "100" g rods. Both sets represent a range of velocities from 1291 m/s to 4525 m/s. All except 1929 have detailed data in the full report [4]. Test 1929 was one of two conducted at R12 and only values given in the published

report are available. Table 1 presents a summary of the experimental conditions listed in the published reference [3].

Table 1.   Experimental Conditions

Case	Rod Radius (cm)	Rod Length (cm)	Rod Mass (g)	Rod Velocity (m/s)
"100" g rods				
1929	0.3435	15.578	100.01	1291
5835	0.3380	15.583	96.96	2653
5839	0.3376	15.583	96.73	3449
"50" g rods				
5841	0.2640	12.179	46.20	2365
5842	0.2635	12.179	46.02	3580
5844	0.2620	12.169	45.41	4525

Computational Tools

CTH Code Features

The CTH [5, 6, 7] code was developed to model a wide range of solid dynamics problems involving shock wave propagation and multiple material motion in one, two, or three dimensions: one-dimensional rectilinear, cylindrical, and spherical meshes; two-dimensional rectangular and cylindrical meshes; and three-dimensional rectangular meshes are available. An explicit two-step Eulerian solution scheme is used with these meshes for each computational cycle. The first step is a Lagrangian step in which the cells distort to follow the material motion. The second step is a remesh step where the distorted cells are mapped back to the original Eulerian mesh.

CTH has several thermodynamic material models that are used for simulating strong shock, large deformation events. Both tabular and analytic equations-of-state are available. CTH can model elastic-plastic behavior, high explosive detonation, fracture, and motion of fragments smaller than a computational cell. A linearly-elastic perfectly-plastic material strength model is available with two yield surface options: a von Mises (constant) yield surface and a pressure dependent yield surface. Both options support thermal softening and low density degradation corrections. Several rate-dependent viscoplastic models are available to treat non-linear yield surface changes. Simple fracture models are available to the user. Both programmed burn models and reaction rate models are available for simulating high explosive detonation. Ideal gas, Jones-Wilkens-Lee and tabular Sesame equations-of-state are available for computing the thermodynamic properties of high

explosive reaction products. A special model is available for moving fragments smaller than a computational cell with the correct statistical velocity.

CTH has been carefully designed to minimize the dispersion generally found in Eulerian codes. It has a high-resolution interface tracker that prevents breakup and distortion of material interfaces. It uses second-order convection schemes to flux all quantities between cells. Information about the particular version of CTH used for these calculations is presented in Appendix A.

ALEGRA Code Features

ALEGRA is a multi-material, arbitrary-Lagrangian-Eulerian (ALE) code for solid dynamics being developed by the Computational Physics Research and Development Department at Sandia National Laboratories [1,2]. It combines the features of modern Eulerian shock codes, such as CTH, with modern Lagrangian structural analysis codes. With the ALE algorithm, the mesh can be stationary (Eulerian) with the material flowing through the mesh, the mesh can move with the material (Lagrangian) so there is no flow between elements, or the mesh motion can be entirely independent of the material motion (Arbitrary). All three mesh types can coexist in the same problem, and any mesh may change its type during the calculation. Material model capabilities in ALEGRA include common equation of state and constitutive models similar to those provided in CTH. Models are available to handle material mechanical properties, fracture, high explosive burn, and thermal conductivity. Information about the particular version of ALEGRA used for these calculations is presented in Appendix A.

Computational Models

CTH Baseline Problem Definition

The impacting rods and target blocks are modeled as axisymmetric objects in two dimensions. While the experiment used threaded tungsten rods in order to sabot launch them from a light-gas gun, smooth rods are used in the simulations, since the size of the threads is well below the resolution of the computational meshes used here. The impacting ends of the rods were treated as flat, while the actual penetrators had rounded, hemispherical ends. The rod lengths used in this study are the same as those from the published data report [3]. The rod radii are computed to be the equivalent radius of a rod with the same length and mass as the actual rod.

A uniform 0.065 cm mesh is used in the central region of the problem where the rod impacts the block and the crater forms. There are 15 radial zones of this size, extending out to a radius of 0.975 cm. The zones then grow with a ratio of 1.025, out to a radial distance of about 29 cm. This large distance is chosen to minimize the potential for reflections from the transmitting boundary condition on the edges of the armor plate region. In the axial direction, the initial position of the rod and most of the armor block are zoned with 0.065 cm mesh, thus giving a uniform two-dimensional mesh in most of the crater formation

region. This uniform mesh extends to a depth of 25 cm for the 100 g rods and a depth of 20 cm for the 50 g rods. The portion of the armor plate below the crater is zoned with mesh that grows at a 1.025 rate, to a total depth of about 31 cm for the 100 g rods and 26 cm for the 50 g rods. Earlier studies of these penetrating rod problems [9, 10] have shown the adequacy of this size mesh to resolve the macroscopic physical processes. Mesh boundary conditions are reflective on the axis of symmetry and transmitting elsewhere (with one exception). The transmitting boundary simulates an infinite medium. The problems were all run to a time of 200 μs. A listing of the CTH input for the 5844 case is shown in Appendix A.

All CTH calculations described here were performed on the DOE Teraflop massively parallel computer on 5/4/97. The 50 g rod calculations used 67158 zones, counting boundary cells and the 100 g rod problems used 81666 zones, including boundary cells. The problems each ran on 64 processors, using about 3 Megabytes of memory per processor. This amount of memory is well below the upper limit and a much smaller number of processors could have been used in these calculations. The execution times of the problems were between 1.5 and 2 hours and the "grind" times ranged from 17 to 19.5 μs/zone-cycle.

ALEGRA Baseline Problem Definition

As with CTH, axisymmetric two-dimensional geometry is used to model the rods and armor plates in ALEGRA. Rods are again modeled as smooth cylinders. While the problem was run with ALEGRA's Eulerian option, the mesh was generated with the Version 2.3X of the FASTQ [8] code and is a body-fitted mesh. This implies that one of the cell boundaries lies exactly on the impacting rod edge, thus eliminating mixed material cells at the edge of the rod, prior to interaction with the plate. Also implied is that the mesh is not exactly uniform, as it is in the CTH case.

The number of radial zones specified in the rod was either 4, for the 50 g rods, or 5 for the 100 g rods. This led to a radial mesh size that varied slightly between the different rods from 0.06426 to 0.06509 cm, but was still, for all purposes, the same as that used in the CTH problem definition. This uniform zoning is carried out to a radius of 1.5 cm, after which the zone size increases at a 1.10 rate, out to a radius of about 30 cm. Zoning in the axial direction in the interaction region where the crater is formed is uniformly 0.065 cm. The incoming rod moves through mesh that increases from 0.065 cm at a rate of 1.10 starting at the top of the armor plate. Zoning in the axial direction below the interaction region increases at a 1.10 rate, to a depth of about 32 cm for the 50 g rod problems and 37 cm for the 100 g problems. The interaction region of uniform axial mesh of size 0.065 cm extends from the surface of the armor plate to a depth of about 21 cm for the 50 g bars and 26 cm for the 100 g rods. The axis of symmetry is defined to be a reflective boundary, with the other boundaries of the problem being transmitting. The problems were all run to a time of 250 μs. Listings of the FASTQ and ALEGRA input setups are shown in Appendix A.

Away from the central interaction region, the zoning for the ALEGRA simulations is graded more coarsely than the CTH zoning. For example, while the CTH problem has the

portion of the rod external to the armor block moving through uniform mesh, the rod in the ALEGRA simulations moves through zones that increase in their axial size as the back of the bar is approached. This choice was made to produce a smaller problem size and thus allow scoping calculations with ALEGRA to be done on workstations. The mesh was carried forward into the final set of calculations since no problems were seen with this approach.

The six ALEGRA problems were all run on the DOE Teraflop Computer on 5/2/97. The 50 g rod problems employed 25263 elements, while the 100 g rod problems used 30429 elements. These values are smaller than the number of zones used in the CTH calculations because the ALEGRA mesh was graded in the radial direction with a larger ratio (1.10 versus 1.025) than the CTH mesh, resulting in fewer zones needed to span the armor block. A larger ratio was also used in the vertical direction for the region above the armor block and in the deepest sections of the block. The problems were decomposed for multiprocessor computation using version 2.02 of the NEM_SLICE code. The problems all ran on 16 processors and took between 3 and 6 hours of wall clock time each to complete. At the time of these runs, ALEGRA "grind" times were not available.

Computational Models

Both our ALEGRA and CTH calculations use Mie-Gruneisen forms for the equation of state (EOS) of both tungsten alloy and rolled armor. A linear relationship between shock-velocity and particle velocity is assumed. A von-Mises yield surface with thermal softening and density degradation is used for material strength. The parameters of these models are presented in Table 2. Parameters for the EOS for the tungsten alloy are taken

Table 2.   EOS and Material Model Parameters

Parameter	Tungsten Alloy	Armor Plate
Density (g/cm^3) ρ_0	17.346	7.85
Sound Speed (cm/s) c	4.035×10^5	3.574×10^5
S	1.24	1.92
Γ_0	1.67	1.69
C_V (ergs/ev)	1.75×10^{10} (CTH), 1.57×10^{10} (ALEGRA)	5.18×10^{10} (CTH) 5.17×10^{10} (ALEGRA)
Y (kbar)	18	7.5
Poisson's Ratio, ν	0.28	0.33
Young's Modulus (ALEGRA only) (Mbar)	1.02	3.72
Fracture Stress (kbar)	-18 (CTH) -6 (ALEGRA)	-20 (CTH) -15 (ALEGRA)

5

from Steinberg [14] for 95W-3.5Ni-1.5Fe. The Poisson's ratio of 0.28 is consistent with Steinberg's initial shear modulus of 1.45, and the yield strength of 18 kbars is close to the value of 18.7 in [14]. Note, however, that these experimental results were obtained using Kennametal W10 alloy, which is 90W-7Ni-3Fe. Strength properties are often sensitive to details of metallurgical composition and we simply used the best information available to us at the time these runs were performed. Reference [3] gives the compressive yield strength at 0.2% offset of 174 ksi, or 12 kbar, and 13.2 kbar at 1.0% offset. A yield strength that is too large in the tungsten alloy would result in penetrations that are too deep. The Young's modulus (YM) value is only specified in the ALEGRA setups and can be derived from the Poisson's ratio and the other constants $(YM = 3(1-2v)\rho_0 c^2)$. The value used here is consistent with these other values.

Note also that a different specific heat was inadvertently used by the two codes, due mainly to the input being in two different units for C_V: ergs/K for ALEGRA and ergs/ev for CTH. This small difference causes no significant difference in the results of these calculations as was verified by making an ALEGRA run of case 5841 with the CV value used by CTH. While the fracture pressure limits were inadvertently made different, there was no evidence of fracture in the problems run. There are cases where the fracture modeling plays a key role, such as for penetration of finite width plates. The ALEGRA features that made this so are discussed more below.

Parameters for the RHA EOS are identical to the standard CTH Mie-Gruniesen library values for iron and are identical to those listed in the standard LANL hugoniot reference [15]. The yield strength and Poisson's ratio are identical to those used in an earlier comparison of CTH results with these experimental results [10] and these values were in turn taken from the Metals Handbook [16], given the Brinell hardness number values for the RHA bars cited in [3].

For CTH, the two dimensional mesh had the left side as a symmetry boundary, the bottom side as an extrapolated pressure boundary, and the top and right sides as transmitting boundaries. The bottom boundary is a void interface for the entire duration of the problem run. Figure 1 shows a schematic of the mesh layout used in these calculations. The multiple material temperature and pressure thermodynamics model (MMP) was used which allows each material in a computational cell to have a separate temperature and pressure. Velocity was advected to conserve momentum and excess kinetic energy was discarded. The "high resolution" (SMYRA) interface scheme was used to track material interfaces. In mixed material cells, the yield strength was calculated from a volume averaged value normalized by the sum of the volume fractions of the materials in the cell that could support shear. For fracture modeling, a principal stress comparison with the specified fracture stress value is used to test for fracture. In mixed material cells, no fracture was allowed, by setting the fracture stress to a very large negative value. The same condition was used in cells that contain void. The von Mises constant yield surface model was used, with the default melting temperature of 0.13 eV and the default value of α, the fraction of the melt temperature where material begins to lose strength, of 0.8.

Transmitting Boundary

Rolled
Homogeneous
Armor

Symmetry (Reflective) Boundary

Transmitting Boundary

Tungsten Penetrator

Void

Extrapolated Pressure Boundary
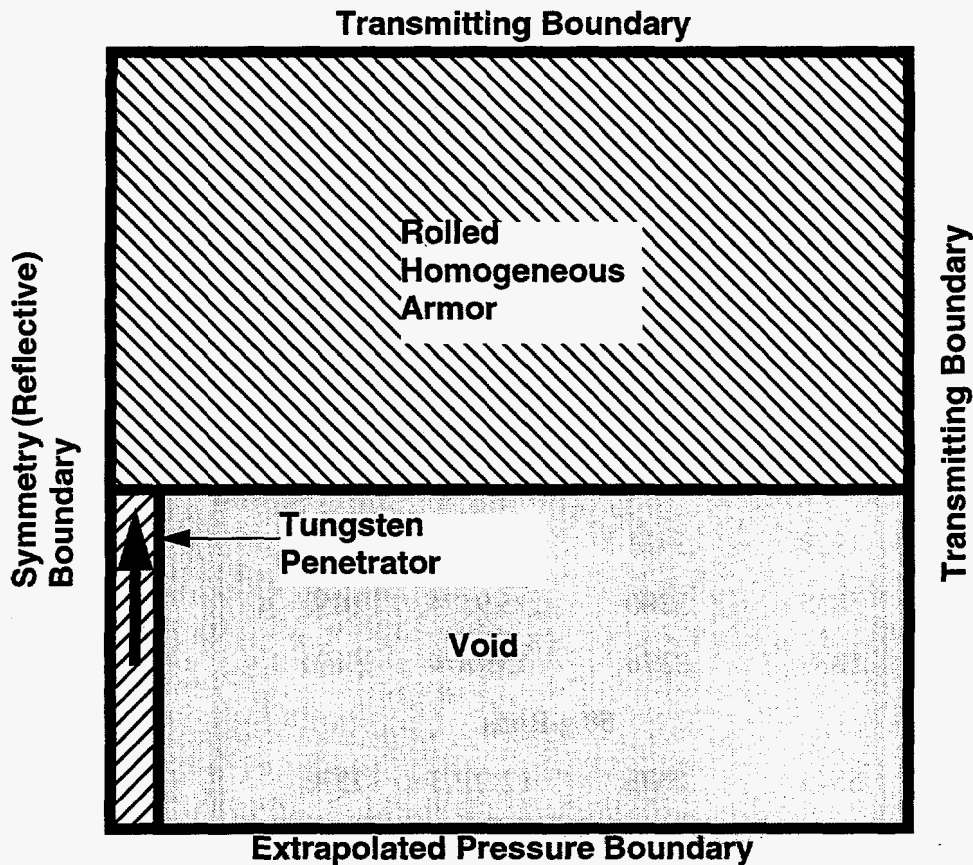
Figure 1.   Schematic of the CTH mesh used in these calculations.

For ALEGRA, the parameter that controls the number of Lagrangian steps to take for each Eulerian remap is set to one, so the code runs in a pure Eulerian form just as CTH. ALEGRA is also set to do just one remapping in every remesh step. The SMYRA interface tracker is used, the Pisces hourglass control is set at 0.05, a time step is used that is 0.9 of the stability limit and the set of nodes along the axis of symmetry is set for no displacement in the radial direction. The nodes along the sides of the mesh that encompass the void region from which the rod is impacting the plate are set to be a voided side set, the equivalent of the void interface in CTH. While ALEGRA treats mixed cell yield strength the same way as in CTH, there is no equivalent of the mixed material void cell treatment in CTH. In addition, ALEGRA does not currently offer the option of a principal stress criterion for fracture.

The fracture model ("frac presdep") compares the pressure in the cell with the specified fracture pressure and, if the pressure is less, introduces enough void into the cell to bring the pressure back to the fracture pressure. The model specifications in ALEGRA were ordered such that the EOS model is computed first, followed by the elastic-plastic model and then the fracture model. As a result of this ordering, the "pressure" in the cell is set equal to the mean stress. As later discussion will show, stress waves traveling in the tungsten rod are in a state of uniaxial stress, equal to the yield stress, and thus the pressure

7

will be about 6 kbar. Thus, the fracture pressure limit was not exceeded in the ALEGRA runs and no evidence of fracture was seen.

Problem Parameters

The problem setups used in the CTH and ALEGRA runs employed dimensions of the rods that differ slightly from those in the experimental setup. Table 3 shows these parameters. Table 4 shows these parameters for the CTH simulations. The differences arose in the

Table 3.   ALEGRA Rod Parameters

Case	Radius (cm)	Length (cm)	Velocity (m/s)
100 g Rods			
1929	.3433	15.9574	1290
5835	.3380	15.9574	2650
5839	.3376	15.9574	3450
50 g Rods			
5841	.2638	12.2217	2370
5842	.2633	12.2217	3580
5844	.2633	12.2217	4525

Table 4.   CTH Rod Parameters

Case	Radius (cm)	Length (cm)	Velocity (m/s)
100 g Rods			
1929	.3435	15.575	1290
5835	.3380	15.575	2650
5839	.3376	15.575	3450
50 g Rods			
5841	.2638	12.18	2370
5842	.2633	12.18	3580
5844	.2615	12.18	4525

course of building the code input decks. These small differences have negligible impact on the results of the simulations. For example, the CTH run for case 5839 was repeated with

8

a rod length of 15.9574 cm, the value used in the ALEGRA runs. Results were only negligibly different than the baseline results, one of many such sensitivity results that could be pursued by an ambitious reader.

Description of Results

The six rod impact cases described in Table 1 were simulated with both CTH and ALEGRA. The runs were done on both single workstations and the DOE Teraflop massively parallel computer. Figure 2 presents a series of views of the progression of the formation of the penetration channel from ALEGRA for test 5844. Four times are presented with the left side of each panel showing the armor material and the right side showing the tungsten rod material. The lower right panel is at a time that represents the final result. Figure 3 shows a similar result for the CTH simulation.

Channel Depth

Experimental values for channel depth are given in the published report of the experiment [3] and the full data package [4]. Measurements were made on sectioned halves of the armor plates. Depth was measured to the bottom of any residual penetrator that remained in the channel. While experimental errors were not available in the data, photos included in [4] allow an estimate of the roughness of the bottom of the channel and thus an estimate for potential error or variability in the experimental result. These errors are included in the experimental column of Table 5.

Channel depth measurements for the calculational results are made by examining material interface plots available from the post-processing graphics tools available for both CTH and ALEGRA output. These tools represent the material distribution within the mixed material Eulerian cells. For CTH, the CTHPLT [11] tool is used to generate a display such as that shown in Figure 4. This simulation is for the 5841 run. Also displayed on the view is the Eulerian mesh, indicating the resolution used to run the calculation. The material regions are labeled. This section of the problem is the bottom of the channel after the penetration has completed, at a time of 200 μs. The material interface lines drawn on this plot by CTHPLT correspond to the 0.5 contour level of volume fraction. While these lines cross cells, providing the promise of sub-mesh size resolution of the material interface, positions of interfaces in this report are conservatively estimated with errors of plus or minus one cell dimension.

For ALEGRA, the MUSTAFA [12] display tool is used to generate a material interface plot. An example is shown in Figure 5. MUSTAFA's display represents Eulerian cells as being composed of armor (light grey in Figure 5), tungsten rod material (dark grey) or void (black) depending on which has the greater mass fraction in the cell. The material interface is not tracked across the cell. Also presented in Figure 5 is the Eulerian mesh used for the ALEGRA calculation. As one can see, these plots allow location of the interface of the materials to within a zone. Conservatively, the error on the interface location is estimated as plus or minus one zone, which for these simulations equates to approximately ± 0.1 cm.
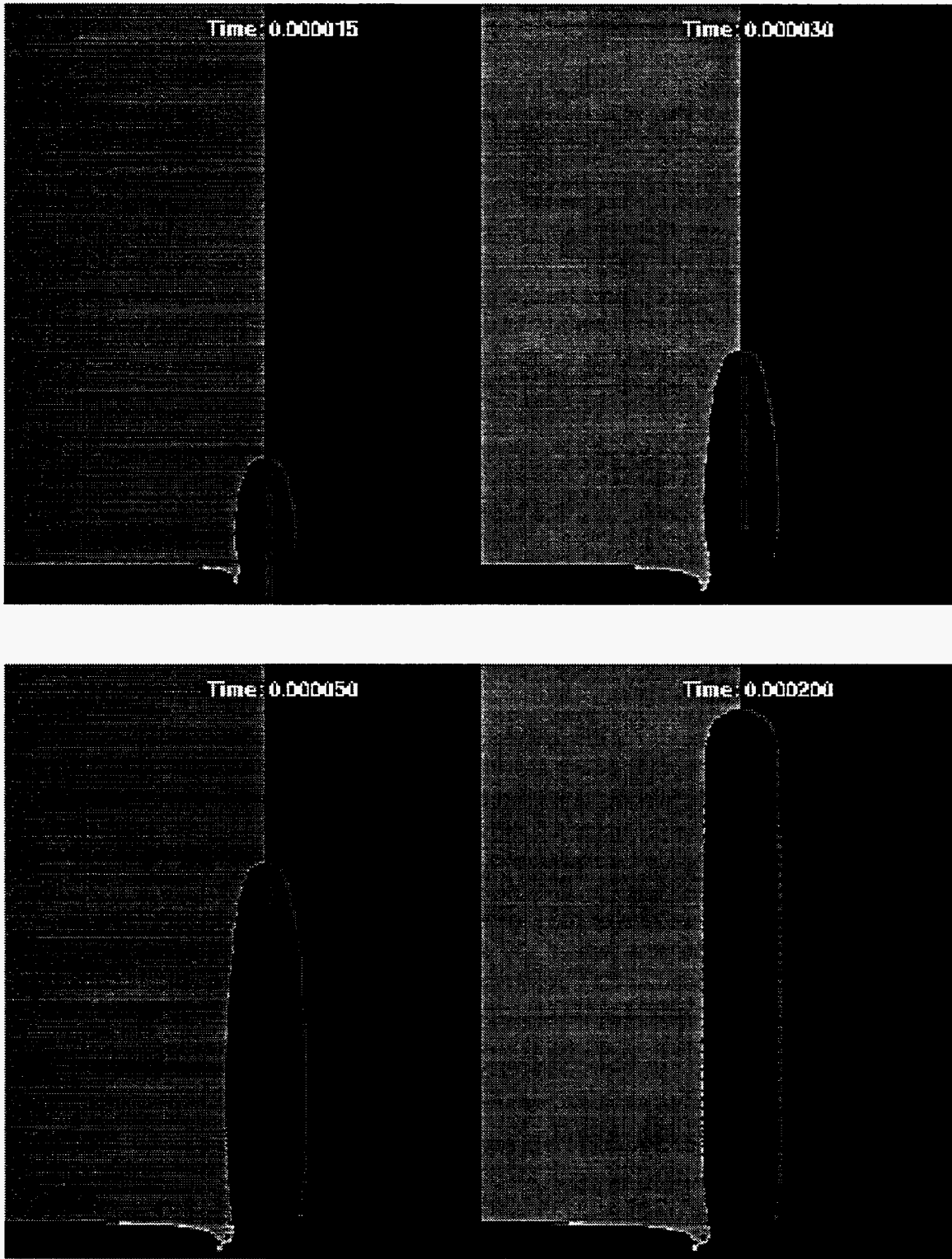
Figure 2.   Simulation results from ALEGRA for the 5844 test case. Material on the left in each frame is armor plate, while the right hand material is tungsten rod. Problem times are 15 μs, 30 μs, 50 μs and 200 μs.
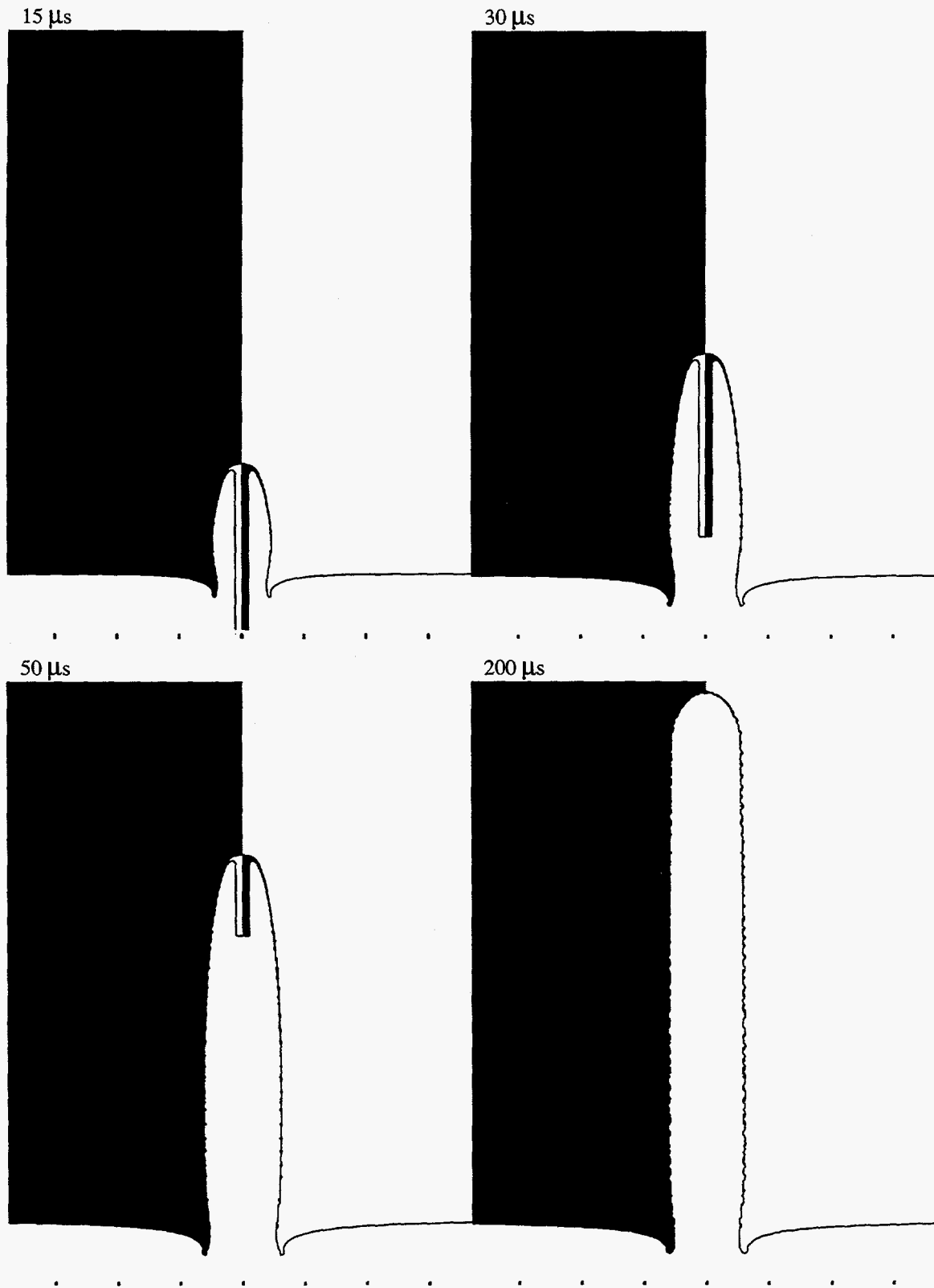
Figure 3. Simulation results from CTH for the 5844 test case. Material on the left in each frame is armor plate, while the right hand material is tungsten rod. Problem times are 15 μs, 30 μs, 50 μs and 200 μs.
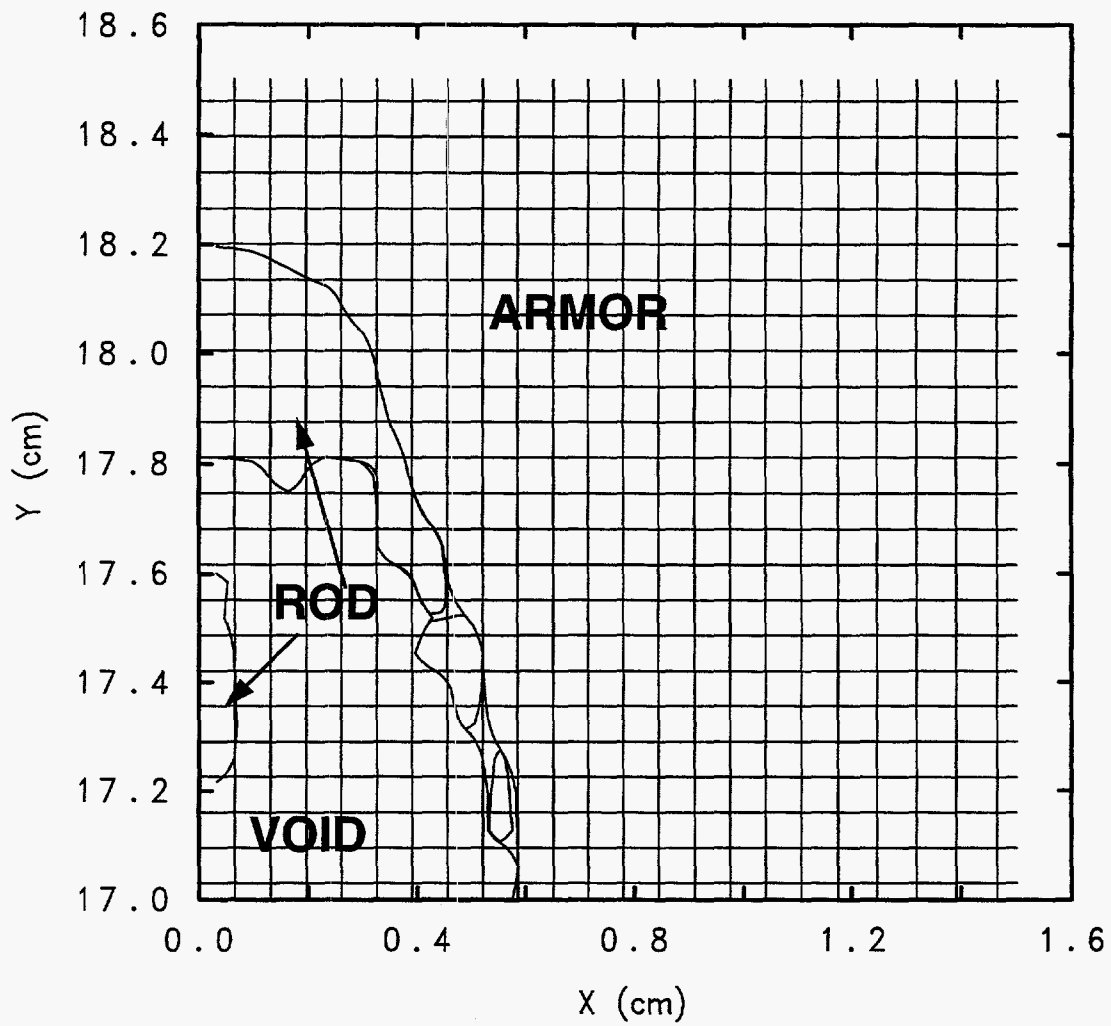
Figure 4.   CTHPLT display of material interfaces for rod impact experiment 5841. The materials are labeled as to their type. Rectilinear black lines on the plot delineate the mesh boundaries for the Eulerian mesh used in the calculation. This result is at a time of 200 μs.
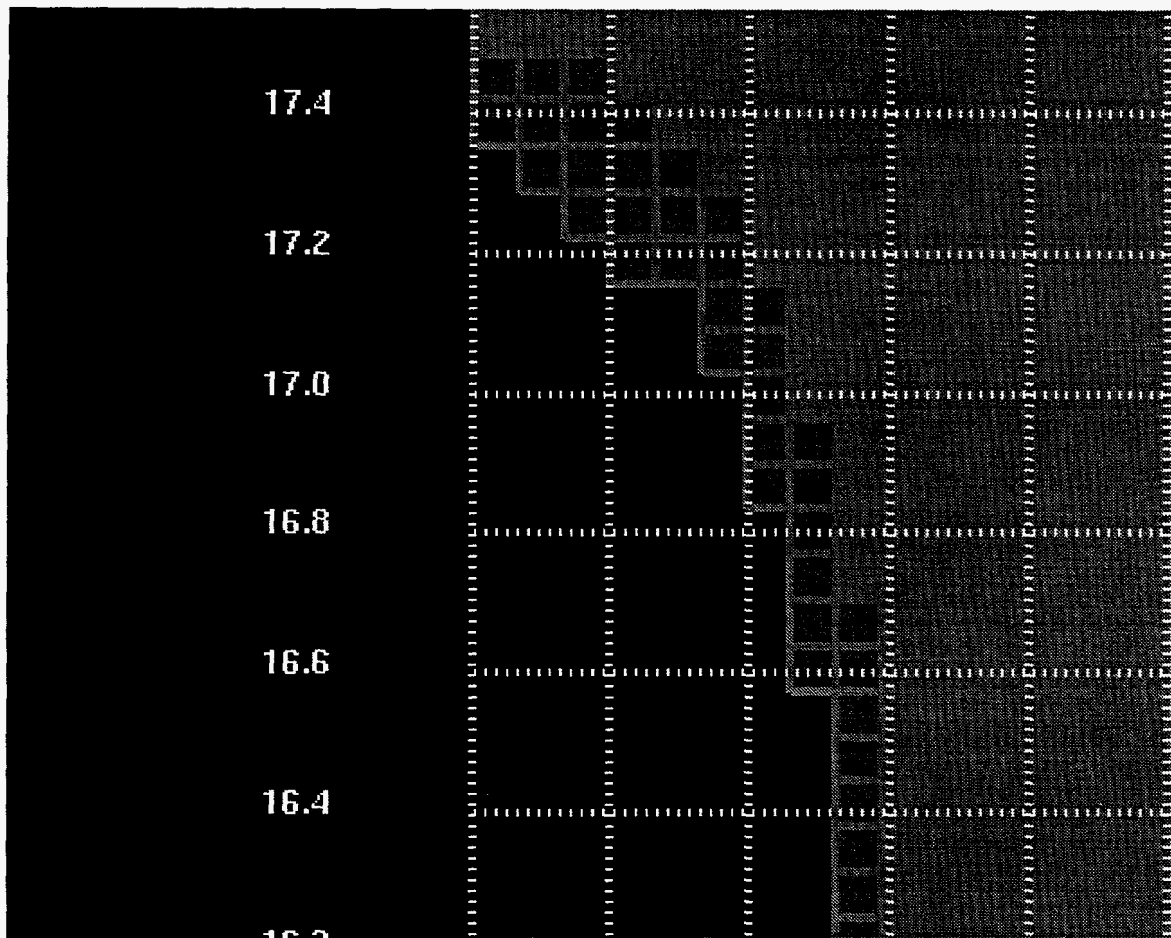
Figure 5. MUSTAFA material interface display for rod impact experiment 5841. Lighter grey represents armor plate, darker grey represents tungsten rod material and black is void. Grey lines on the plot delineate the mesh boundaries for the Eulerian mesh used in the calculation. This result is at a time of 200 μs

Simulation of Armor Penetration by Tungsten Rods

Using this sort of information, Table 5 lists the crater depth results obtained in this study for CTH and ALEGRA. Depths are given in units of centimeters.

Table 5.   Crater Depth Results

Case	Experimental (cm)	ALEGRA (cm)	CTH (cm)
100 g rods			
1929	8.0	8.7 ± 0.07	11.7 ± 0.07
5835	22.85 ± 0.05	23.9 ± 0.07	23.9 ± 0.07
5839	24.15 ± 0.05	24.8 ± 0.07	24.5 ± 0.07
50 g rods			
5841	16.52 ± 0.05	17.5 ± 0.07	18.2 ± 0.07
5842	18.9 ± 0.1	18.8 ± 0.07	19.0 ± 0.07
5844	19.37 ± 0.05	19.2 ± 0.07	19.1 ± 0.07

For two of the cases, a significant portion of tungsten rod remains in the bottom of the channel. One of these cases is 5841, illustrated in Figures 4 and 5. For CTH, the axial length of the remaining plug is 0.4 cm, while for the ALEGRA results, this dimension is about 0.2 cm. Experimentally, there was a plug of penetrator remaining in the bottom of the channel with an axial length of 0.196" or 0.05 cm(Table1.2 [4]).

The other case of remaining penetrator is 1929, where the plug remaining is quite substantial, since the armor plate stopped this slower moving rod before the entire rod erodes onto the walls of the channel. In the CTH runs, a plug of length 1.2 cm remains, while in the ALEGRA runs, the plug length is 1.6 cm. Experimentally, a 1.5 cm length plug remains in the channel [3].

For both 1929 and 5841, the crater depth given in Table 5 is measured to the bottom of the crater eroded into the RHA plate. Thus, the crater depth includes the length of the remaining plug. A graphical representation of the Table 5 results is shown in Figure 6. In this plot, values for CTH and ALEGRA are shifted slightly to the right and left, respectively, to improve visibility of the symbols.

Channel Radius

Experimental values for channel width in the VKG tests were obtained in two ways. One used a tri-point micrometer to take interior measurements of the channel prior to sectioning the armor plate. The second method involved using a snap gauge to take two point measurements of the channel width in the sectioned armor plate. These measurements were obtained at discrete values of depth into the channel. The channels were tapered to varying degrees and thus a range of width was obtained. This experimental range is compared with

Figure 6.   Crater depth results from CTH and ALEGRA, compared to experimental re-
sults. Values for CTH and ALEGRA are shifted slightly to the right and left, respectively,
to improve visibility of the symbols. The case numbers are also shown.

the computational results in Table 6. For the 1929 case, done at R12, there is no such detailed information available, so the single width value given in [3] is used here.

While no experimental errors are cited in this report, one can estimate from photos of the sectioned armor plates a value for surface roughness in the channel. This leads to an estimate of uncertainty in the value of the channel width. These error estimates are included in Table 6. It would be desirable from the view of code validation to have a detailed discussion of experimental error bounds and sources by the original experimenters.

In a manner similar to depth, the computational results for channel radius are read from material interface plots produced from the output of the two codes. As can be seen in Figures 2 and 3 the channel is not of uniform width and thus there is a range of values for channel radius. Radius values are obtained from the location of the inner radial surface of the channel, whether there is armor plate or tungsten alloy present on the channel surface. Error in these values is on the order of the cell size, 0.065 cm, since an interface cannot be located any more precisely than the problem is discretized. This range is comparable to the experimentally reported range. Table 6 presents the results of the simulation runs. Figure 7

Table 6.   Crater Radius Results

Case	Experiment		ALEGRA		CTH	
	Min (cm)	Max (cm)	Min (cm)	Max (cm)	Min (cm)	Max (cm)
"100" g rods						
1929	0.63	0.63	0.45 ± 0.07	0.6 ± 0.07	0.5 ± 0.07	0.65 ± 0.07
5835	0.9 ± 0.1	1.0 ± 0.1	0.95 ± 0.07	1.15 ± 0.07	1.0 ± 0.07	1.2 ± 0.07
5839	1.3 ± 0.1	1.3 ± 0.1	1.25 ± 0.07	1.4 ± 0.07	1.3 ± 0.07	1.6 ± 0.07
"50" g rods						
5841	0.57 ± 0.05	0.71 ± 0.05	0.65 ± 0.07	0.75 ± 0.07	0.65 ± 0.07	0.85 ± 0.07
5842	0.9 ± 0.1	1.01 ± 0.1	1.05 ± 0.07	1.2 ± 0.07	1.05 ± 0.07	1.25 ± 0.07
5844	1.3 ± 0.1	1.5 ± 0.1	1.25 ± 0.07	1.8 ± 0.07	1.3 ± 0.07	1.6 ± 0.07

displays these results graphically. Also in Figure 6, values for CTH and ALEGRA are shifted slightly to the right and left, respectively, to improve visibility of the symbols.

Penetration Velocity

Both CTH and ALEGRA have the capability of placing entities termed "tracer particles" at arbitrary positions within the materials being modeled. These tracers can be either Eulerian, meaning they are fixed in coordinate space, or Lagrangian, which means they move with the material flow in their environment. For these rod impact calculations, a series of Lagrangian tracer particles are placed along the axis of the impacting rod. Information at
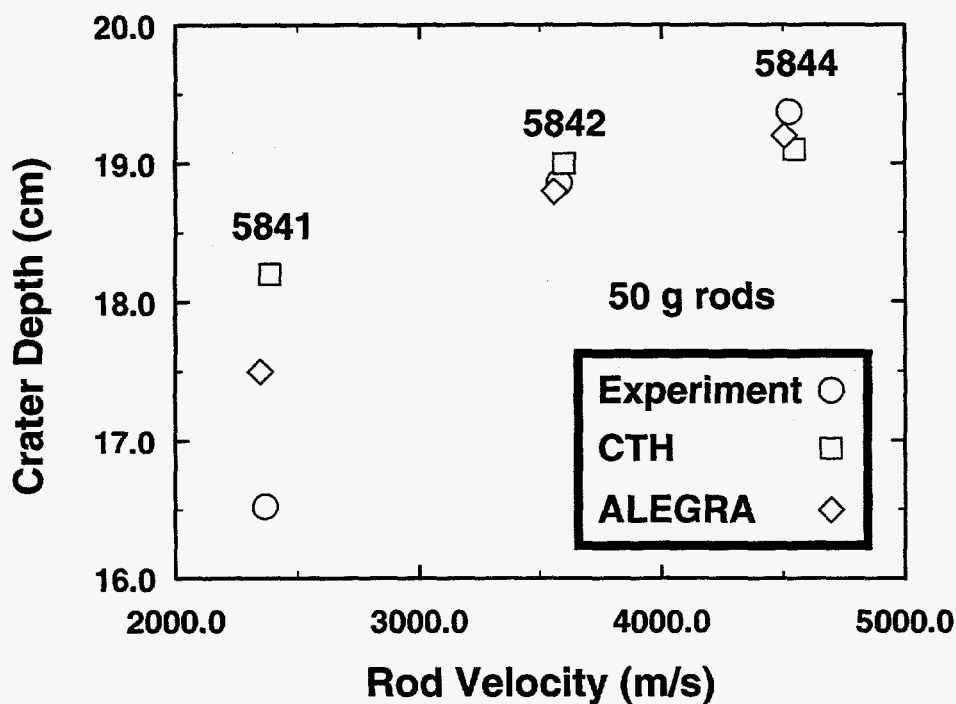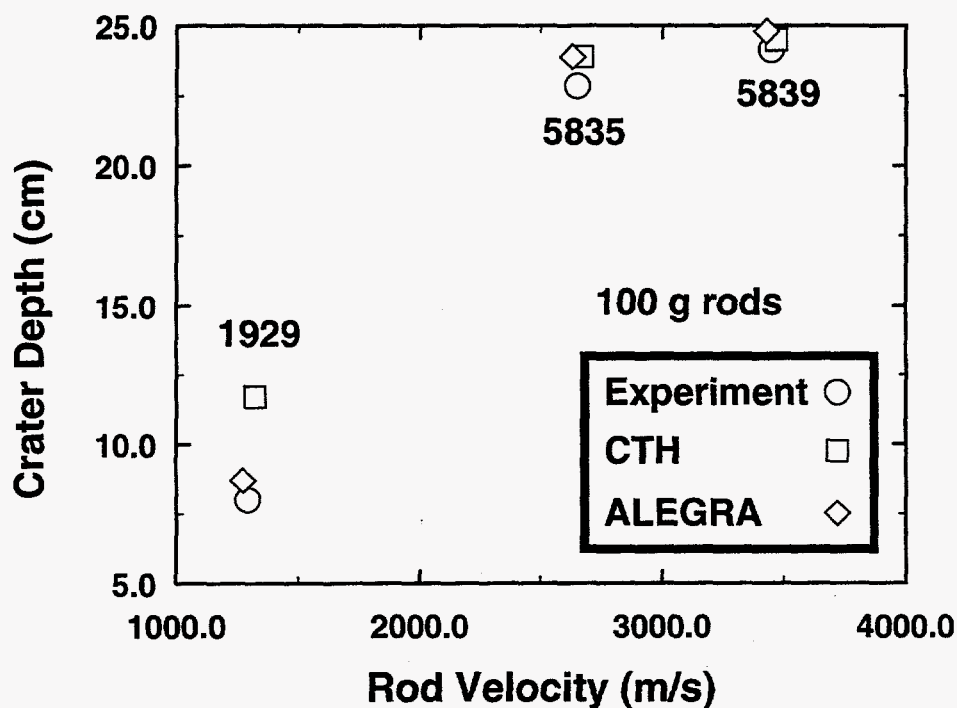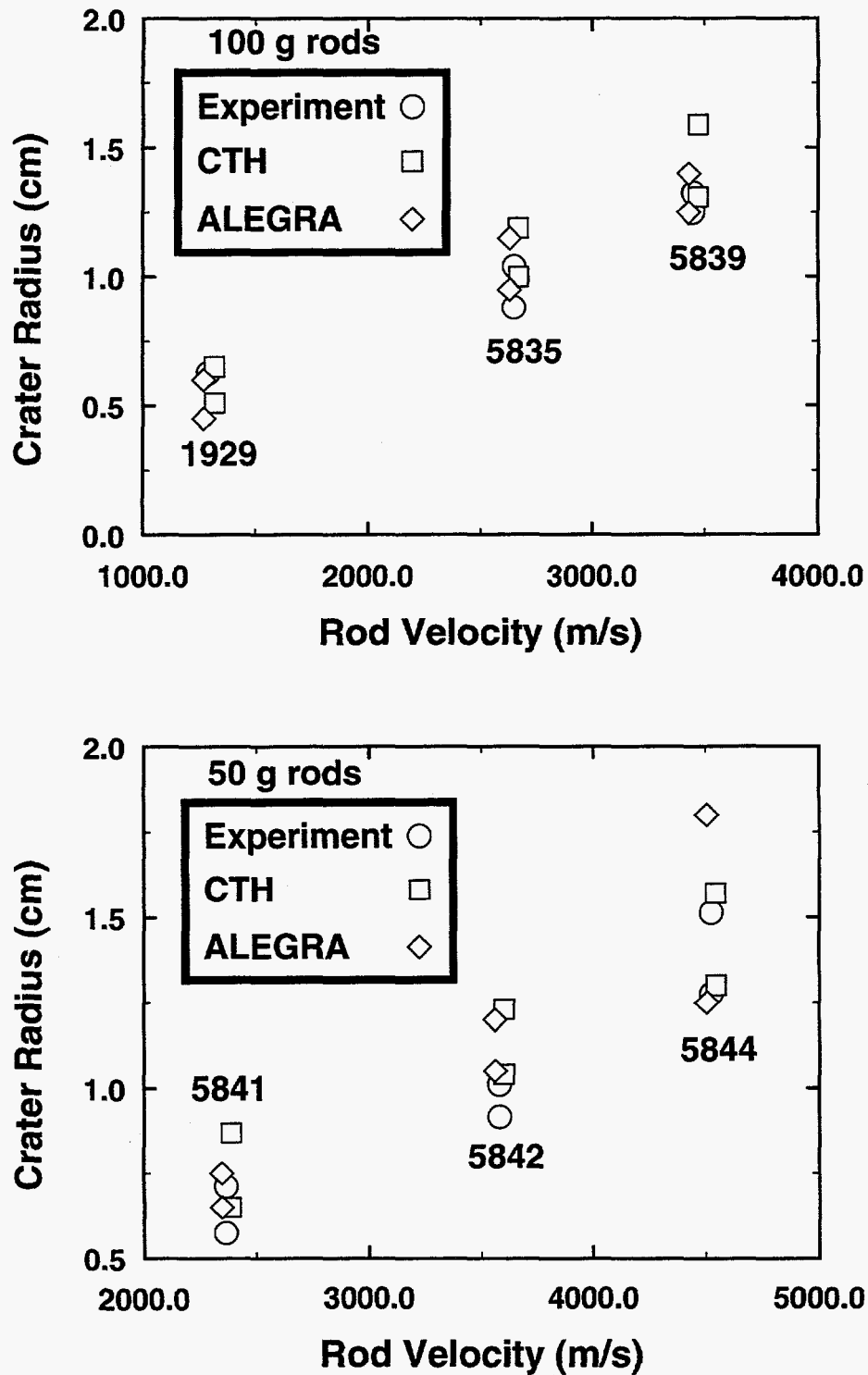
Figure 7. Crater radius results from CTH and ALEGRA, compared to experimental results. Values for CTH and ALEGRA are shifted slightly to the right and left, respectively, to improve visibility of the symbols. Case numbers are also shown.

the tracer points, such as position, velocity, stress are recorded at fixed time intervals and can be examined with the HISPLT [13] post-processing tool.

Figure 8 shows the time history for the ALEGRA tracer particle that starts at an axial position of 5 cm from the armor plate in case 5842. The axial position of the particle is
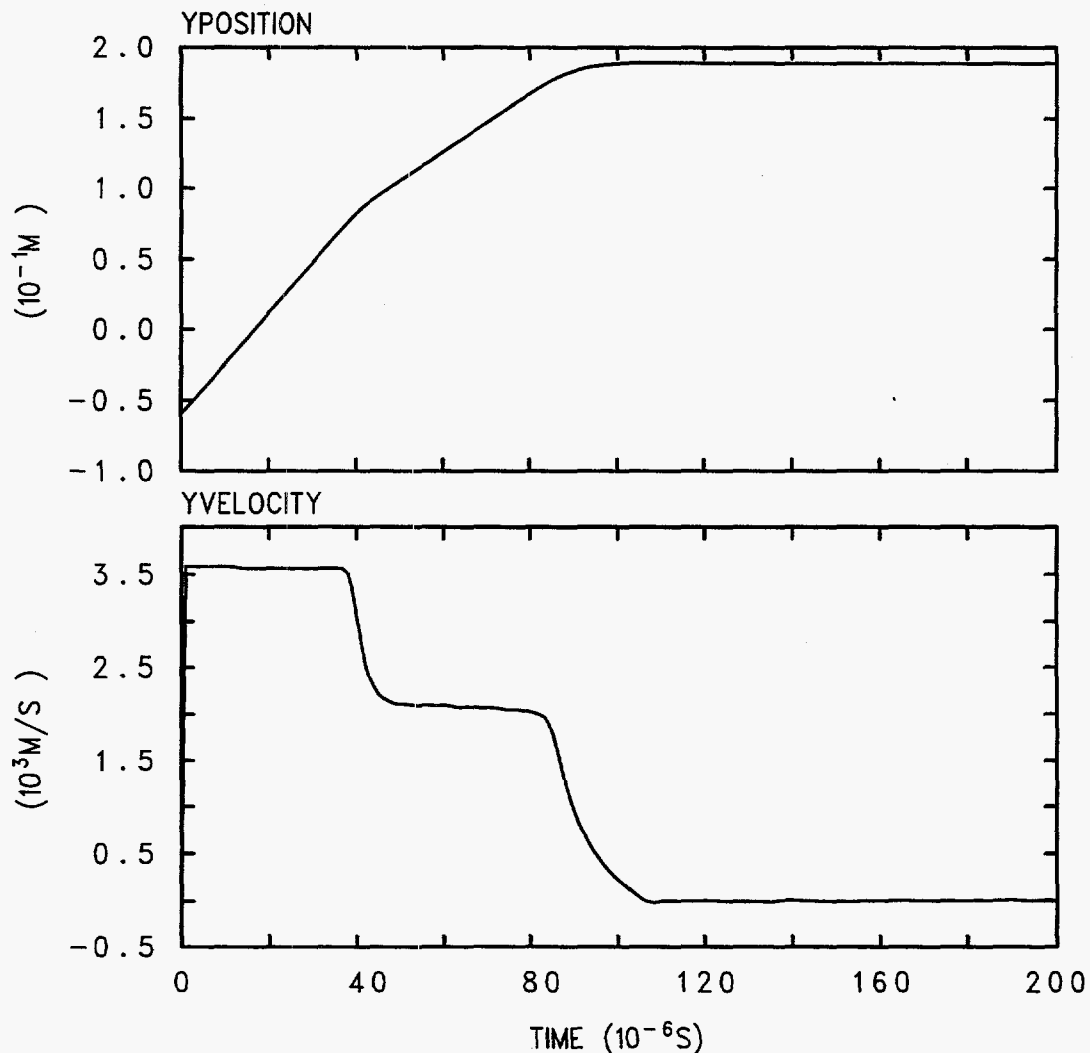
Figure 8.   Time history of axial position and velocity for the ALEGRA lagrangian tracer particle that is initially located 5 cm from the armor plate in problem 5842.

shown in the upper plot, while the axial velocity is shown in the lower plot. Starting with a velocity of 3580 m/s, the particle continues with this velocity until the interaction region with the plate reaches the particle's position, at a time of about 35 μs. The particle velocity then slows to the speed with which the rod is penetrating the armor plate, i.e. the stagnation velocity.

In rods completely consumed by the penetration process, all of the tracer particles eventually find their way to this interaction region. In CTH the tracers were specified to

18

remain on the axis of symmetry; any radial component of velocity was discarded. In ALEGRA, the tracers were free to move off axis. No tracers were observed to migrate away from the axis of symmetry. The tracers arrive at the stagnation point and travel with that point to the bottom of the channel where they eventually stop. For the case shown in Figure 8, this occurs at a time of about 110 μs. A comparable display of the CTH tracer is shown in Figure 9.
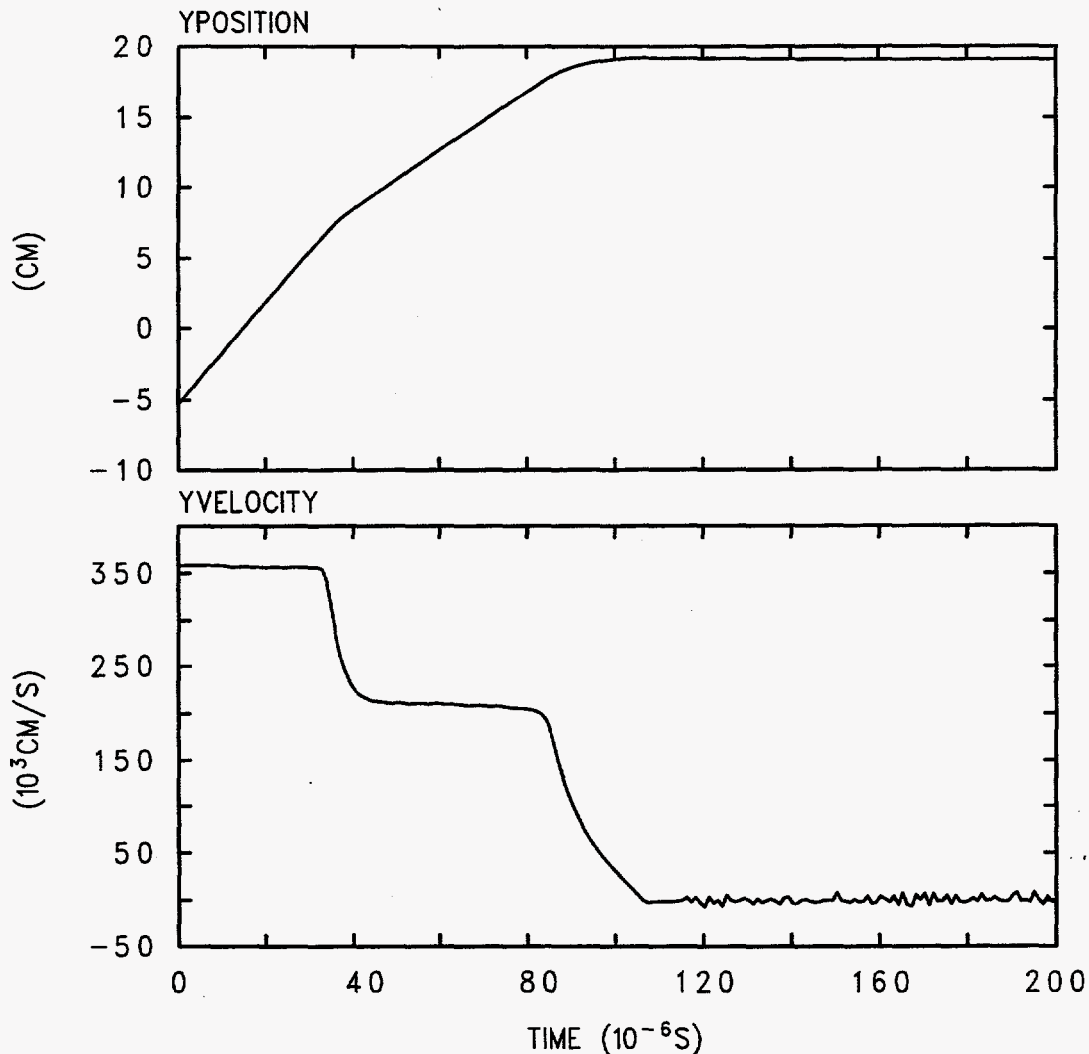
Figure 9.   Time history of axial position and velocity for the CTH lagrangian tracer particle that is initially located 5 cm from the armor plate in problem 5842.

While no experimental results are available for the speed of penetration, analytical models described in [17] can provide an estimate to compare with the results produced by the simulations. This is at least one way of testing the validity of "differential" data emerging from our calculations. For those cases with penetration velocities large enough, the materials behave in a hydrodynamic manner and a simple dynamic pressure balance analysis provides the result to be expected for the speed of penetration and the depth. The tracers that travel along the axis of symmetry should record values of y velocity that are

19

consistent with these calculated values, for those cases in the hydrodynamic limit. The simplest model that ignores any strength properties in the materials, produces an estimate of penetration velocity. With the rod material, of density ρ_r, moving into the interaction region with a relative velocity of $V_r - V_p$, and the RHA material, with density ρ_a, moving into the region with a relative velocity of V_p, the balance of dynamic pressure ρV^2 determines the value of V_p, the penetration or stagnation velocity. One finds

$$V_p = V_r / (1 + \mu), \tag{1}$$

with $\mu = (\rho_a/\rho_r)^{1/2}$. Using a density for armor of 7.85 g/cm^3 and for tungsten of 17.35 g/cm^3, the values shown in Table 7 for stagnation velocity are found. Also shown in Table 7 are

Table 7.   Stagnation Velocities

Case	V_r (m/s)	V_p (m/s)	CTH V_p (m/s)	ALEGRA V_p (m/s)
100 g Rods				
1929	1290	771	650 ± 65	750 ± 65
5835	2650	1584	1550 ± 65	1530 ± 65
5839	3450	2063	2020 ± 65	2020 ± 65
50 g rods				
5841	2370	1417	1320 ± 65	1380 ± 65
5842	3580	2140	2100 ± 65	2090 ± 65
5844	4525	2705	2650 ± 65	2660 ± 65

the measured penetration speeds for the CTH and ALEGRA simulations. A series of measurements on the material interface plots are used to obtain these velocities. The uncertainty in these values is about ± 65 m/s, due to the uncertainty of $\pm$ one-half zone in placing the actual interface position from the material interface plots that have resolution only to the zone size (.065 cm) and are available every 5 μs.

The stagnation velocities are not constant during the interaction, but decrease slightly in steps, due to a decreasing velocity of the rod. Rod velocities decrease due to shock waves that travel back up the rod and release waves that travel from the free end of the rod down to the penetration region. This effect is described in [17] and observable effects in these calculations are described in the next section. The decrease in the stagnation velocity is best seen by viewing in expanded detail the record from an on-axis tracer particle that arrives at the stagnation point and stays there due to the lack of radial velocity on the axis of symmetry. Figure 10 is a time history plot of the y direction velocity at the stagnation point

from the 5842 case calculation by ALEGRA. This tracer is originally located at the
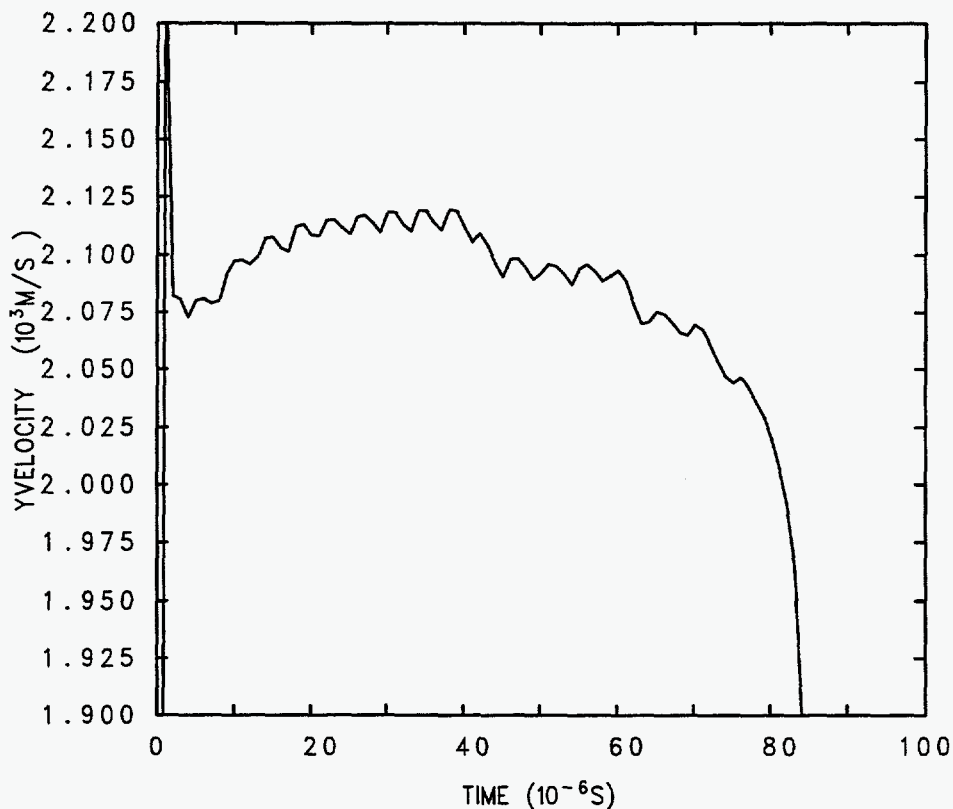
Figure 10.   Time history of the y component of velocity for the ALEGRA tracer particle initially located at the interface between the rod and the armor plate in case 5842.

rod-armor interface and thus shows the transient behavior that occurs while the penetration process becomes quasi-steady. Discernible in this velocity record are at least two distinct values of stagnation velocity: 2115 m/s from 25 to 40 μs and 2090 m/s from 45 to 60 μs. Each of these stagnation velocities is related by the above formula to a reduced rod penetration velocity due to shock and stress waves in the rod.

Shock Wave Propagation in the Tungsten Rod

The rod impact with the armor plate causes a shock wave to travel back along the rod. This shock stresses the tungsten material to its yield strength after which plastic flow will occur. The velocity of the rod towards the interaction region with the plate is decreased behind the shock. When the shock reaches the free end of the rod, a rarefaction wave then travels back down the rod towards the interaction region, relieving the stress caused by the first shock and further reducing the velocity of the rod. Reaching the high pressure region in the interaction zone, where the stress is essentially triaxial and the pressure is about 220 kbar in the 5842 case, the rarefaction reflects as another shock and moves back towards the free end of the rod. The process is repeated as long as there is rod material to support the waves. A sequence of waves runs back and forth along the rod until the rod is consumed by the

penetration interaction region, each complete roundtrip reducing the incoming velocity of the rod by the same amount and thus decreasing the velocity of the interaction region.

The speed of the shock can be estimated with the shock jump equation. A schematic of the wave process is shown in Figure 11. In the frame of the laboratory, a one-dimensional
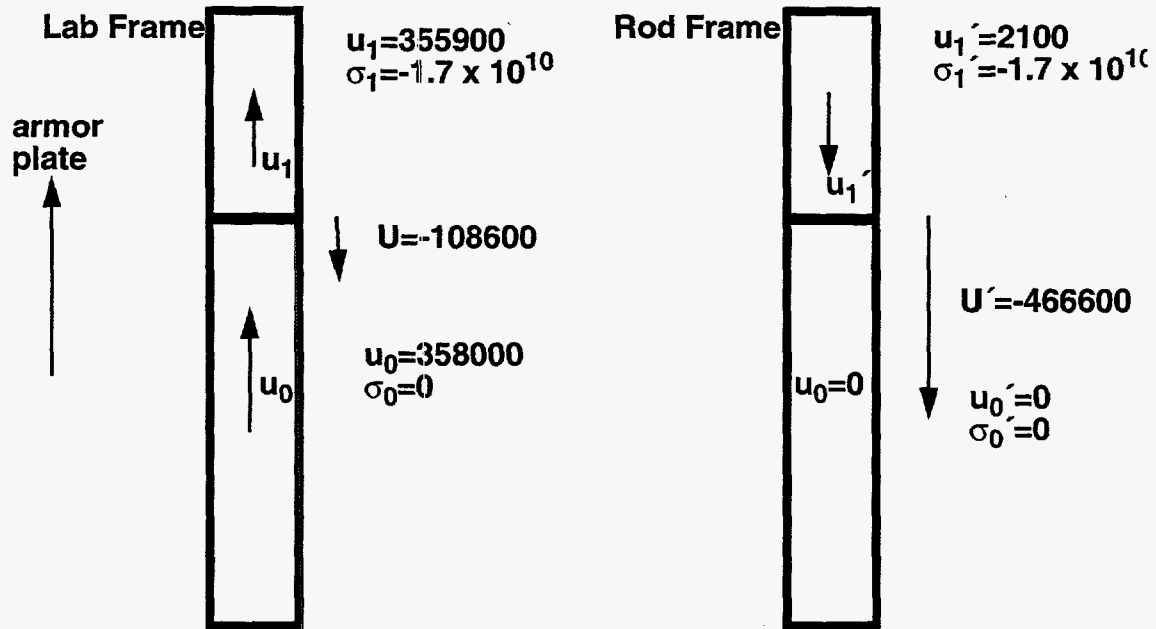
Figure 11. Schematic showing the two different views of the shock wave propagating in the rod towards the free end. Values are from the ALEGRA simulation of case 5842.

shock travels with a constant speed of U towards the free end of the rod, while the rod is moving upward with a speed of u_0. The conditions behind the shock (on the interaction region side) have a particle velocity of u_1, towards the armor plate but of a magnitude less than u_0, and a stress of σ_1. The shock is propagating into unstressed rod material with a particle velocity of u_0. The density ρ_0 is 17.35 g/cm^3. In the rod's rest frame, the shock moves towards the free end with speed U', into an unstressed region with particle velocity $u_0'=0$. Behind the shock, the particle velocity is $u_1'=u_1-u_0$ and the stress is $\sigma_1'=\sigma_1$. The shock jump equation is

$$\sigma_1' - \sigma_0 = \rho_0 \, (u_1' - u_0') \, (U' - u_0'). \qquad (2)$$

Thus U', the speed of the shock in the rod frame, is

$$U' = \sigma_1' / (\rho_0 u_1') \qquad (3)$$

In the laboratory frame, the shock speed is $U = U' + u_0$.

By examining the profiles of stress and y velocity along the axis of the impacting rod, consistency with these jump conditions can be checked. To illustrate this, we do this for one case, 5842. Figure 12 presents profiles of the stress and y velocity as computed by ALEGRA for two times, 15 and 20 μs. Figure 13 presents similar results from CTH. Since CTH computes the stress deviators and the hydrostatic pressure, p, these values are shown. Examination of the ALEGRA results shows that u_0 is 3.580 x 10^5 cm/s as expected from the problem definition, while u_1 = 3.558 x 10^5 cm/s. These values are also noted on the schematic, Figure 11. The stress behind the front, σ_1 is equal to -1.7 x 10^{10} dynes/cm^2. Equation 3 then gives U´= -4.666 x 10^5 cm/s as the propagation speed of the shock back up the rod in the rod frame and -1.09 x 10^5 cm/s in the laboratory frame. Thus the shock appears to move relatively slowly towards the back end of the rod. The measured shock speed from Figure 12 is -1 ± 0.065 x 10^5 cm/s, consistent with the above calculations.

Each interaction of the wave with the free end of the rod or the penetration region causes a decrease in rod velocity of the same magnitude as the first shock wave, 0.021 x 10^5 cm/s. These decreases can be seen in the later wave profiles that are for a time after that shown in Figure 12. Table 8 shows the rod velocities that result, and for every other rod velocity, the penetration velocity implied by the hydrodynamic pressure balance expression, equation 1. These values match the values seen in Figure 10 and other tracer histories.

One obvious feature of the profiles shown in Figures 12 and 13 are the oscillations about the mean values behind the wave front. While these could be due to effects related to the use of artificial viscosity in these shock physics codes, these oscillations may also be legitimate features of the stress history in the rod, due perhaps to interactions with the free surface of the rod and the off-axis regions of the interaction region. This work has not explored this possibility. Another area that has not been examined is the difference in stress and pressure profiles between ALEGRA and CTH.
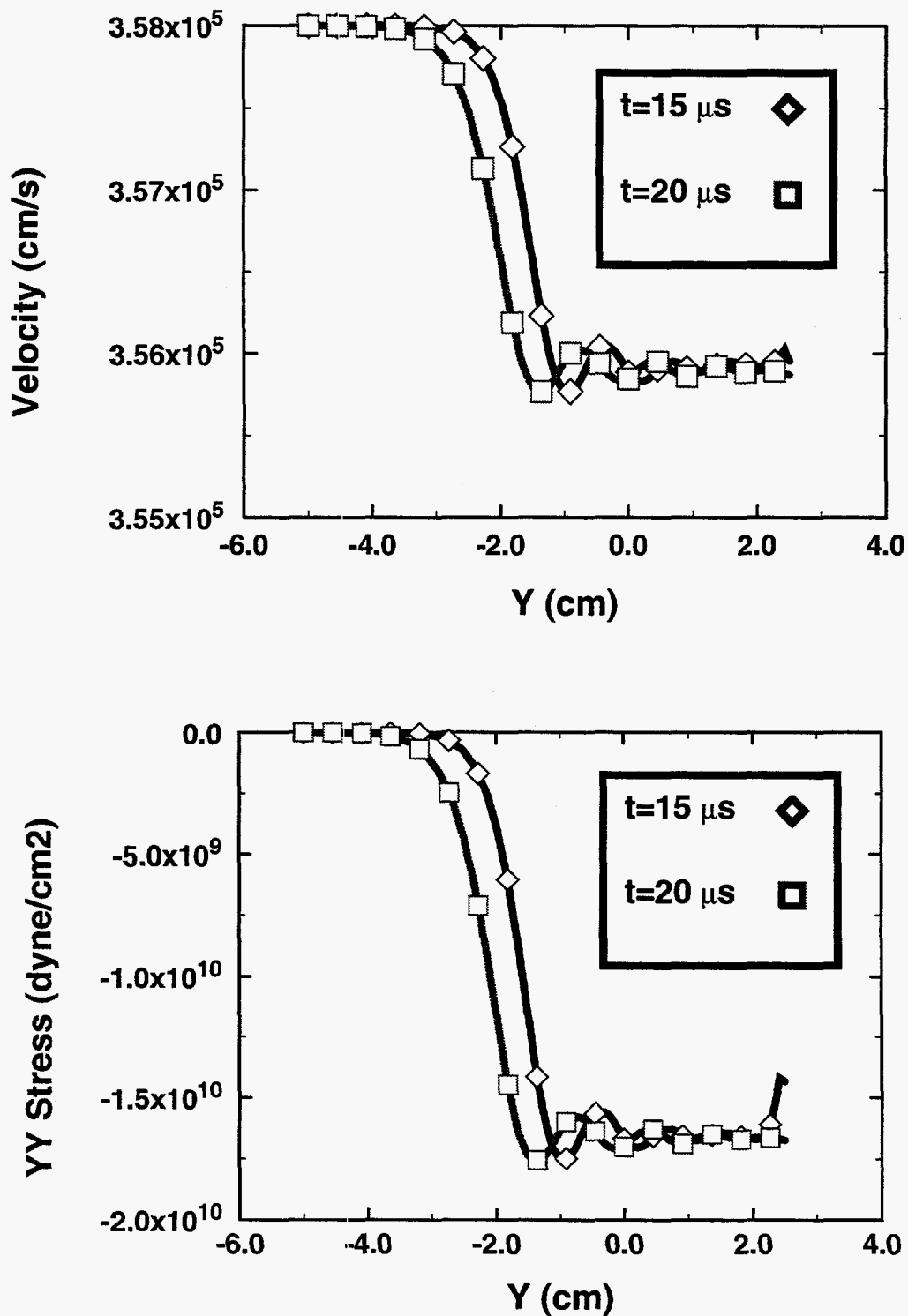
Figure 12. Profiles of the Y component of velocity and the YY component of stress along the axis of the rod from the ALEGRA calculation of case 5842 at times of 15 and 20 μs.
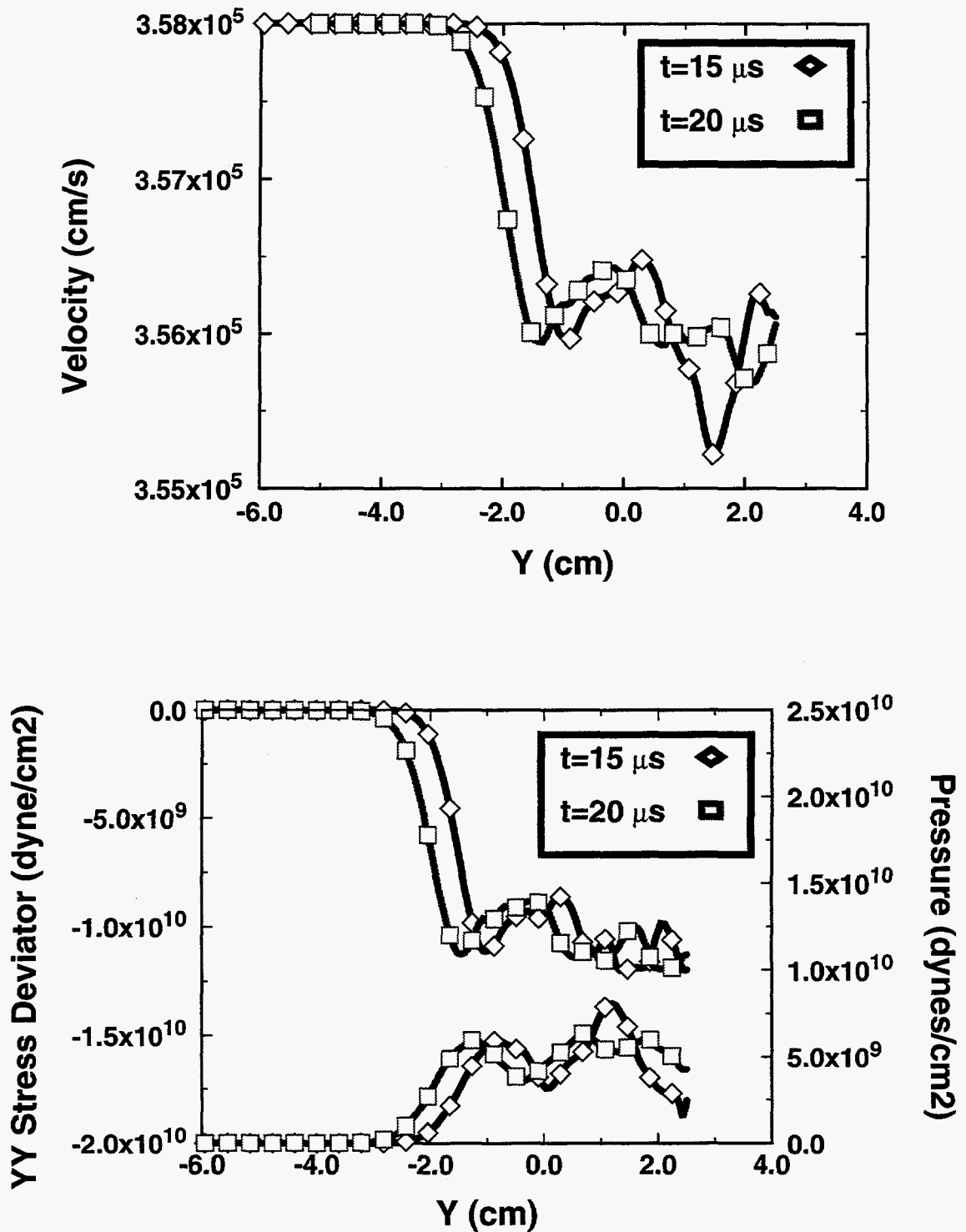
Figure 13. Profiles of the Y component of velocity and the YY stress deviator and pressure along the axis of the rod from the CTH calculation of case 5842 at times of 15 and 20 μs.

Table 8. Wave effects on Rod Velocity, Case 5842

Rod Velocity (cm/s)	Penetration Velocity (cm/s)
3580	2140
3559	
3538	2115
3517	
3496	2090
3475	
3452	2064

Discussion

For most of the results shown here, simulations by both ALEGRA and CTH show very good agreement with one another and with the experimental data. With the exception of the CTH simulation of the slowest penetrating rod, case 1929, values for channel depth produced by both CTH and ALEGRA are within 10% of the experimental results and often within a few percent. The 1929 CTH channel is 46% too deep. While Figure 5 makes the error appear large for case 5841, the CTH channel is only 10% too deep, while the ALEGRA result is too deep by only 6%. Simulated results for channel radius range are very close to measured values. Errors are always less than 20%, but in these cases this is only 2 to 4 times the experimental error or the error in assigning a location to the interface calculated by the code. Both codes tend to overpredict the channel width. We do not address the ultimate origins of this problem in this paper.

Case 1929 is the slowest rod penetration case in this set and results in the largest plug of rod material remaining in the channel. It is likely that behavior of this case is strongly linked to modeling of strength in both the armor plate material and the tungsten rod. As described in [17], once the rod velocity approaches or falls below a limiting value, strength properties of the two materials lead to widely differing forms of results for total penetration results and the time evolution of the penetration. While both the ALEGRA and CTH codes have more sophisticated strength models available, this initial study did not probe their applicability and performance. This will be an area of future work.

Examination of the details of the problem have shown that there exists a wealth of observables that can be compared to simple theoretical predictions. Wave speeds in the tungsten rod, variations in the stagnation velocity and the coupling of these speeds to the

wave phenomenon in the rod and other similar phenomena can be compared to expected behavior and agreement assessed. Agreement in these details lends support to the use of these computational tools in more complex cases. In addition, the observed oscillatory behavior of the state behind the shock traveling up the rod shows that complex behavior related to interaction with the side of the rod can also be investigated and compared to more detailed models of the rod-armor interaction.

Future work will include systematic parameter variations from the baseline problems described here. Parameters for the strength models and the EOS models will be investigated for their effects on the results. Differences in the computational mesh will be looked at, with an emphasis to exploring the effect of the new tiling algorithm approach to building computational meshes. This is a major issue in testing the utility of such meshes for shock dominated calculations. The use of the ALE methods employed in ALEGRA will also be tried, both single material ALE (SMALE) and multi-material ALE (MMALE). New ALEGRA capabilities for automatic mesh refinement will be explored also. While this study made use of earlier work that determined an acceptable mesh size for this type of problem, mesh convergence studies will be revisited.

Conclusion

This report presents comparisons between experimentally determined results from the penetration of long tungsten alloy rods into rolled armor plates and computer simulations of the same events. Results obtained with the ALEGRA and CTH codes, using both workstation networks and the massively parallel Teraflop computer to perform the calculations, show that both codes produce results that are, for the most part, within a few percent of experimental measurements of penetration channel width and depth. Other shock physics phenomena observed in the results also match expected behavior and lend support to the use of these computational tools in modeling complex material interactions.

References

[1]Summers, R. M., Peery, J., Wong, M. W., Hertel, E. S., Trucano, T. G., Chhabildas, L. C., "Recent Progress In ALEGRA Development and Application to Ballistic Impact," Proceedings of the 19th HyperVelocity Impact Symposium, 1996.

[2]Budge, K. G., Peery, J. S., Robinson, A. C., Summers, R. M., Wong, M. K., "ALEGRA: User Input and Physics Descriptions," to be published, Sandia National Laboratories, Albuquerque, NM, 1997.

[3]Silsby, G. F., "Penetration of Semi-Infinite Steel Targets by Tungsten Long Rods at 1.3 to 4.5 km/s," Proceedings of the ADPA Eighth International Symposium on Ballistics, Orlando, Florida, October 1984.

[4]Blanks, J. R., "Ballistic Research Lab KE Penetrator Impact Test," September 1983, Private communication to Paul Yarrington, Org. 9232, Sandia National Laboratory.

[5]Hertel, E. S., Bell, J. L., Elrick, M. G., Farnsworth, A. V., Kerley, G. I., McGlaun, J. M., Petney, S. V., Silling, S. A., Taylor, P. A., Yarrington, L. "CTH: A Software Family for Multi-Dimensional Shock Physics Analysis," Proc. 19th International Symposium on Shock Waves, Vol. 1, p.377, July 1993.

[6]McGlaun J. M., Thompson, S. L., Kmetyk, L. N., Elrick, M. G., "CTH: A Three-Dimensional ShockWave Physics Code." Int. J. Impact Engng., 10:351, 1990

[7]McGlaun, J. M., Thompson, S. L., and Elrick, M. G., "A Brief Description of the Three-Dimensional Shock Wave Physics Code CTH." SAND89-0607, Sandia National Laboratories, Albuquerque, NM, 1989.

[8]Blacker, T. D., "FASTQ Users Manual Version 1.2," SAND88-1326, Sandia National Laboratory, Albuquerque, NM, July 1988.

[9]Hertel, E. S., "A Comparison of Calculational Results with Experimental Data for Long Rod Projectiles," SAND90-0610, Sandia National Laboratories, Albuquerque, NM, December 1990.

[10]Kmetyk, L. N., Yarrington, P., "Cavity Dimensions for High Velocity Penetration Events - A Comparison of Calculational Results with Data," SAND88-2693, Sandia National Laboratories, Albuquerque, NM, May 1989.

[11]Elrick, M. G., "CTHPLT User's Guide and Input Instructions, Version 3.00," July 12, 1996.

[12]Glass, M. W., "MUSTAFA User's Guide, Version 1.0," March, 1997.

[13]Thompson, S. L., Kmetyk, L. N., "HISPLT - A Time-History Graphics Postprocessor User's Guide," SAND91-1767, Sandia National Laboratories, Albuquerque, N.M., September 1991.

[14]Steinberg, D. J., "Equation of State and Strength Properties of Selected Materials," Lawrence Livermore National Laboratory, UCRL-MA-106439, Change 1, February 13, 1996.

[15]GMX-6, "Selected Hugoniots," LA-4167-MS, Los Alamos National Laboratory, May 1, 1969.

[16]Metals Handbook, Volume 1, Properties and Selection of Metals, American Society for Metals, 8th Edition, 1961, p. 1234.

[17]Zukas, J. A., "High Velocity Impact Dynamics," John Wiley & Sons Inc., 1990.

APPENDIX A

Computer Code Details

1. CTH Version

The version of the CTH code used for all these calculations was identified as being last modified on 2/25/97. The versions of the major packages in the code is shown in the following Table.

Table A-1. CTH Package Version Identification

CTH package - latest modification date	02/25/97>
AUXILARY FUNCTION package 1.07.a	08/07/89>
CONVECTION package 1.08.a	01/01/92>
CTH EXECUTIVE ROUTINES package 1.08.r	06/05/95>
DATABASE MANAGER package 1.07.c	06/20/94>
EDIT ROUTINES package 1.07.m	02/25/97>
ENERGY BALANCE package 1.09.a	12/18/96>
EULERIAN REZONE package 1.08.j	04/21/94>
HISTORY EDIT package 1.07.j	10/21/96>
LAGRANGIAN STEP IN EULERIAN CODE package 1.08.l	06/05/95>
MESH ACTIVATION package 1.07.c	1/29/91>
SCRATCH DATABASE MANAGER package 1.07.g	11/10/94>
TIMESTEP package 1.07.f	06/05/95>
TRACER PARTICLE ROUTINES PACKAGE 1.07.i	03/09/92>
USER INPUT PACKAGE 1.08.q	12/10/96>
VELOCITY ADDITION package 1.07.d	12/13/93>
DISCARD package 1.00.f	02/01/95>
BIT FUNCTION package	7/10/89>
DATA BASE MANAGER package	12/09/96>
ENERGY BALANCE package 1.09.a	12/18/96>

Table A-1. CTH Package Version Identification

CTH package - latest modification date	02/25/97>
ENERGY SOURCE package	07/10/96>
HE BURN package	1/17/97>
TABLE package	04/16/96>
UTILITY package	02/01/96>
ELASTIC-PLASTIC package 2.06	04/04/95>
EOS package	07/25/96>
SESAME EOS subpackage	07/25/96>
ANEOS subpackage	04/11/96>
MULTIPHASE package 1.01	03/27/95>
EXTRA VARIABLE package 1.09	03/31/92>
INTERFACE TRACKING package 1.09.d	04/21/94>
DDCOMP/Auto-Rezone package	06/14/96>
MULTI PROCESSOR (NX) package 1.00	02/24/97>
INTERRUPT and LIST routines	12/09/96>
INTERNAL STATE VARIABLE INTERFACE package	3/31/95>
UNIX (TFLOP) package	9/05/96>
DEVELOPER1 package 0.00.a	00/00/00>
DEVELOPER2 package 0.00.a	00/00/00>
HEAT CONDUCTION package 1.02.a	11/29/95>
VIRTUAL OBJECTS package 1.10	07/30/96>

2. CTH Input for Experiment 5844 Simulation

```
************************************************************
*
*  2d long-rod penetration calculation
*
************************************************************
*
*eor* genin
*
************************************************************
*
*  title record
*
```

```
Armor Penetration Test VKG 5844
*
***********************************************************************
*
*   control records
*
control
  mmp
endc
*
***********************************************************************
*
*   mesh records
*
mesh
*
  block 1   geom=2dc   type=e
*
    x0  0.0
      x1   n=15   dxf=0.065   w=0.975
      x2   n=100   dxf=0.065   r=1.025
    endx
*
    y0  -13.0
      y1   n=508 dyf=0.065 w=33.02
      y2   n=50   dyf=0.065 r=1.025
    endy
*
    xact    0.0 0.3
    yact  -13.0 0.0
*
  endb
*
endm
*
***********************************************************************
*
*   material insertion records
*
insertion_of_material
*
  block 1
*
    package w penetrator
      material 1
      numsub 50
      yvelocity 4.525e5
      insert box
        p1   0.0      -12.18
        p2   0.2615   0.0
      endi
    endp
*
    package armor plate
      material 2
      numsub 50
      insert box
        p1   0.0    0.0
        p2 100.0 100.0
```

31

```
        endi
      endp
*
    endb
*
endi
*
************************************************************************
*
*  tracer records
*
tracer
 block 1
    add 0.0 -12.0 to 0.0 0.0 n=10   fixed=x
 endb
endt
*
************************************************************************
*
*  new eos records
*
eos
*
* tungsten mie-gruneisen
*
   mat1   mgrun   ro=17.346   cs=4.035e5   s=1.24
                  go=1.67     cv=1.746e10
*
* steel mie-gruneisen
*
   mat2   mgrun   ro=7.85    cs=3.574e5    s=1.92
                  go=1.69    cv=5.183e10
*
ende
*
************************************************************************
*
*  material strength records
*
epdata
  matep 1   yield=18.0e9   poisson=0.28
  matep 2   yield=7.5e9    poisson=0.33
  mix 3
ende
*
************************************************************************
*
*eor* cthin
*
************************************************************************
***
*
*  title record
*
Armor Penetration Test VKG 5844
*
************************************************************************
*
*  control records
```

```
*
control
  tstop=200.0e-6
endc
*
***********************************************************************
*
*  cell thermodynamics records
*
cellthermo
  mmp
  ntbad=999999
endc
*
***********************************************************************
*
*  convection records
*
convct
  convection=1
  interface=high
endc
*
***********************************************************************
*
*  fracture records
*
fracts
  stress
  pfrac1 -18.0e9
  pfrac2 -20.0e9
  pfmix  -1.0e12
  pfvoid -1.0e12
endf
*
***********************************************************************
*
*  edit records
*
edit
*
  shortt
    time=0.0   dt=1.0
  ends
*
  longt
    time=0.0   dt=1.0
  endl
*
  restt
    time=0.0   dt=1.0
  endr
*
  plotdata
    volume
    stress
    mass
    energy
    temperature
```

```
      endp
*
   plott
      time=0.0   dt=5.0e-6
   endp
*
   histt
      time=0.0   dt=1.0e-6
      htracer all
   endh
*
ende
*
**********************************************************************
*
*   boundary condition records
*
boundary
   bhydro
      block 1
         bxbot=0
         bxtop=1
         bybot=2
         bytop=1
      endb
   endh
endb
*
**********************************************************************
*
*eor* pltin
*
```

3. FASTQ Input for Mesh Generation for Experiment 5844 Simulation

```
TITLE
ALE/EUL- Silsby Test 5844 fq mesh 2 (50g/4.525km/s) 4/27/97
POINT     1         0.0                -12.2217
POINT     2         0.2633             -12.2217
POINT     3         1.50               -12.2217
POINT     4         28.80835           -12.2217
POINT     5         0.0                0.00
POINT     6         0.2633             0.00
POINT     7         1.50               0.00
POINT     8         28.80835           0.0
POINT     9         0.0                20.995
POINT    10         0.2633             20.995
POINT    11         1.50               20.995
POINT    12         28.80835           20.995
POINT    13         0.0                25.63618
POINT    14         0.2633             25.63618
POINT    15         1.50               25.63618
POINT    16         28.80835           25.63618
POINT    17         0.0                31.68711
POINT    18         0.2633             31.68711
POINT    19         1.50               31.68711
POINT    20         28.80835           31.68711
LINE      1   STR      1      2    0      4   1.0000
LINE      2   STR      2      3    0     19   1.0000
LINE      3   STR      3      4    0     40   1.1000
LINE      4   STR      5      6    0      4   1.0000
LINE      5   STR      6      7    0     19   1.0000
LINE      6   STR      7      8    0     40   1.1000
LINE      7   STR      9     10    0      4   1.0000
LINE      8   STR     10     11    0     19   1.0000
LINE      9   STR     11     12    0     40   1.1000
LINE     10   STR     13     14    0      4   1.0000
LINE     11   STR     14     15    0     19   1.0000
LINE     12   STR     15     16    0     40   1.1000
LINE     13   STR     17     18    0      4   1.0000
LINE     14   STR     18     19    0     19   1.0000
LINE     15   STR     19     20    0     40   1.1000
LINE     16   STR      5      1    0     48   1.0500
LINE     17   STR      5      9    0    323   1.0000
LINE     18   STR      9     13    0     22   1.1000
LINE     19   STR     13     17    0      8   1.1000
LINE     20   STR      6      2    0     48   1.0500
LINE     21   STR      6     10    0    323   1.0000
LINE     22   STR     10     14    0     22   1.1000
LINE     23   STR     14     18    0      8   1.1000
LINE     24   STR      7      3    0     48   1.0500
LINE     25   STR      7     11    0    323   1.0000
LINE     26   STR     11     15    0     22   1.1000
LINE     27   STR     15     19    0      8   1.1000
LINE     28   STR      8      4    0     48   1.0500
LINE     29   STR      8     12    0    323   1.0000
LINE     30   STR     12     16    0     22   1.1000
LINE     31   STR     16     20    0      8   1.1000
REGION    1      1     -4    -21    -7     -17
REGION    2      1     -5    -25    -8     -21
REGION    3      1     -6    -29    -9     -25
REGION    4      1     -7    -22   -10     -18
```

```
REGION        5        1       -8      -26      -11      -22
REGION        6        1       -9      -30      -12      -26
REGION        7        1      -10      -23      -13      -19
REGION        8        1      -11      -27      -14      -23
REGION        9        1      -12      -31      -15      -27
REGION       10        2       -1      -20       -4      -16
REGION       11        3       -2      -24       -5      -20
REGION       12        3       -3      -28       -6      -24
SCHEME     0 M
BODY        1 2 3 4 5 6 7 8 9 10 11 12
NODEBC        1       16       17       18       19
ELEMBC        1        1        2        3       28
ELEMBC        2       13       14       15       31       30       29
EXIT
```

4. ALEGRA Version

The version of ALEGRA used in these calculations is generically 3.1. The particular code was built on 4/19/97, using the 1.3-3a Release of the Teraflop cross-compiler iCC on the SUN LAN. The environment variable ALEGRA_CODE was set to "alegra", meaning that only the physics options related to solid dynamics were included in the code. The ALEGRA_DIM variable was set to "2D" and ALEGRA_MP was set to "mp_nx", indicating that the NX message passing library was used in the code. The use of these variables is explained in the ALEGRA User's Manual [2].

5. ALEGRA Input for Experiment 5844 Simulation

```
title
ALE/EUL- Silsby Test 5844 pfcv3 fine (50g/4.525km/s) 4/27/97

physics: solid dynamics
cylindrical

MAXIMUM INITIAL TIME STEP 1.e-10

termination time 250.0e-6

$read restart 69.83E-6

emit output: time        = 5.0e-6, from 0.0 to 1.0
emit plot: time          = 5.0e-6, from 0.0 to 1.0
$emit restart: time       = 20.0e-6, from 0.0 to 20.E-6
$emit restart: time       = 2.0e-6, from 20.0E-6 to 30.E-6
emit restart: time       = 30.0e-6, from 0.0 to 1.0
emit hisplt: time        = 1.0e-6, from 0.0 to 1.0

plot variable
 pressure: avg
 stress: avg
 strain: avg
 velocity
 energy
 density: avg
 temperature: avg
end

domain
  smyra interface tracker
  interior mesh iterations 1
  voided side set 1
end

time step scale:
  hydro 0.9
  strain softening 0.9
end

pisces hourglass control
  viscosity 0.05
end

$barton artificial viscosity
$    linear 0.1
$    quadratic 2.0
$end

no displacement: nodeset 1 x

tracer points
  lagrangian tracer 1 x 0.0    y -0.0
  lagrangian tracer 2 x 0.0    y -3.0
  lagrangian tracer 3 x 0.0    y -3.75
  lagrangian tracer 4 x 0.0    y -6.0
  lagrangian tracer 5 x 0.0    y -7.5
```

```
   lagrangian tracer 6 x 0.0     y -9.0
   lagrangian tracer 7 x 0.0     y -11.25
   lagrangian tracer 8 x 0.0     y -11.75
   lagrangian tracer 9 x 0.0     y -12.0
   lagrangian tracer 10 x 0.171    y -0.0
   lagrangian tracer 11 x 0.171    y -3.0
   lagrangian tracer 12 x 0.171    y -3.75
   lagrangian tracer 13 x 0.171    y -6.0
   lagrangian tracer 14 x 0.171    y -7.5
   lagrangian tracer 15 x 0.171    y -9.0
   lagrangian tracer 16 x 0.171    y -11.25
   lagrangian tracer 17 x 0.171    y -11.75
   lagrangian tracer 18 x 0.171    y -12.0
end

block 1
  eulerian mesh
  material 1
  remesh frequency 1
$  angle trigger 0.0
end

block 2
  eulerian mesh
  material 2
  remesh frequency 1
$  angle trigger 0.0
end

block 3
  eulerian mesh
  remesh frequency 1
$  angle trigger 0.0
end

initial block velocity: block 2, Y 4.525E5

material 1         $ RHA
  model  = 1
  model  = 2
  model  = 3
  init density 7.85   $g/cm3
  init temperature 298.0 $kelvin
end

$constitutive 1 hydrodynamic
model 2 elastic plastic
    youngs modulus     1.02e+12 $ dyne/cm^2
    poissons ratio     0.33
    yield stress       7.5e+9  $ dyne/cm^2
    hardening modulus 0.0
    beta 1.0
end

model 1 mg us up
  c0             3.574e5
  s1             1.920
  gamma0         1.69
  cv             4.46e6
```

39

```
    rho ref            7.85
    pref               0.0
    tref               298.0
    pressure cutoff    -5.0e10
  end

  model 3 frac presdep
    $init frac stress = -2.0e10
    init frac pres = -1.5e10
  end

  material 2         $ Tungsten alloy
    model  = 4
    model  = 5
    model  = 6
    init density 17.346   $g/cm3
    init temperature 298.0 $kelvin
  end

  $constitutive 2 hydrodynamic
  model 5 elastic plastic
      youngs modulus       = 3.72e+12     $ dyne/cm^2 y=3(1-2nu)rc**2
      poissons ratio       = 0.28
      yield stress         = 18.0e+09   $ dyne/cm^2
      hardening modulus    = 0.0        $ dyne/cm^2
      beta                 = 1.
  end

  model 4   mg us up
    c0               4.03e5
    s1               1.24
    gamma0           1.67
    cv               1.35e6
    rho ref          17.346
    pref             0.0
    tref             298.0
    pressure cutoff  -5.0e10
  end

  model 6 frac presdep
    init frac pres = -6.0e09
    $init frac stress = -1.8e10
  end

  exit
```

40

Distribution

EXTERNAL DISTRIBUTION

Allahdadi, Firooz (3)
Phillips Laboratory
PL/WSSD
Kirtland AFB, NM 87117-6008
Attn: F. Allahdadi, D. Medina, & J.
Thomas

Anderson, Charles E. (3)
Southwest Research Institute
P.O. Drawer 28510
San Antonio, TX 78284
Attn.: C. Anderson, D. Littlefield, J. D.
Walker

Ari, Nasit (3)
Kaman Sciences Corporation
1500 Garden of the Gods Road
P. O. Box 7463
Colorado Springs, CO 80933
Attn: Nasit Ari, Sheldon Jones, J. Secary

Christiansen, Eric L. (2)
NASA Johnson Space Center
Space Science Branch - Mail Code SN3
Houston, TX 77058
Attn: E. Christiansen & J. Kerr

Fahrenthold, Eric P.
Department of Mechanical Engineering
The University of Texas
ETC 5.160
Austin, TX 78712

Johnson, Gordon R.
Alliant Techsystems Inc. (MN11-1614)
600 2nd Street NE
Hopkins, MN 55343

Kimsey, Kent
AMSRL-WT-TC
Army Research Laboratory

Aberdeen Proving Ground, MD 21005-5066

Mair, Hans (3)
Institute for Defense Analysis
Operational Evaluation Division
1801 North Beauregard Street
Alexandria, VA 22311-1772

Los Alamos National Laboratory
Mail Station 5000
P.O. Box 1663
Los Alamos, NM 87545

Attn: T. F. Adams, MS F663
Attn: S. T. Bennion, MS F663
Attn: D. E. Burton, MS-F663
Attn: R. J. Bos, MS D406
Attn: M. W. Burkett, MS G787
Attn: T. Dey, MS F665
Attn: J. K. Dienes, MS B216
Attn: R. Gustavsen, MS P952
Attn: B. L. Holian, MS J569
Attn: K. S. Holian, MS B221
Attn: J. W. Hopson, MS B216
Attn: J. Mace, MS C920
Attn: D. Mandell, MS F663
Attn: R. Scammon, MS C931
Attn: R. Wittaker, MS F665

University of California
Lawrence Livermore National Laboratory
7000 East Ave.
P.O. Box 808
Livermore, CA 94550

Attn: R. B. Christensen, MS L-035
Attn: C. McMillan, MS L-035
Attn: W. Moran, MS L-200
Attn: M. J. Murphy, MS L-368
Attn: J. E. Reaugh, MS L-290
Attn: R. E. Tipton, MS L-035

Sandia Internal

MS:	Attention:
0318	G. S. Davidson, 9215
0321	W. J. Camp, 9200
0439	D. R. Martinez, 9234
0441	G. S. Heffelfinger, 9226
0819	E. A. Boucheron, 9231
0819	K. G. Budge, 9231
0819	D. E. Carroll, 9231 (20)
0819	M. A. Christon, 9231
0819	M. G. Elrick, 9231
0819	E. S. Hertel, 9231 (10)
0819	J. S. Peery, 9231
0819	S. V. Petney, 9231
0819	A. C. Robinson, 9231
0819	R. M. Summers, 9231
0819	T. G. Trucano, 9231 (10)
0819	J. R. Weatherby, 9231
0819	M. K. Wong, 9231
0820	P. Yarrington, 9232
0820	R. L. Bell, 9232
0820	R. M. Brannon, 9232
0820	H. E. Fang, 9232
0820	A. V. Farnsworth, 9232
0820	M. E. Kipp, 9232
0820	S. A. Silling, 9232
0820	P. A. Taylor, 9232
0821	M. B. Boslough, 9233
0834	A. C. Ratzel, 9112
0834	M. R. Baer, 9112
1109	A. L. Hale, 9224
1110	D. S. Greenberg, 9223
1111	S. S. Dosanjh, 9221
1168	T. Bergstresser, 9322
1181	J. Asay, 9575
1181	L. C. Chhabildas, 9575
1187	M. K. Matzen, 9571
1187	T. A. Haill, 9571
1187	M. R. Douglas, 9571
1187	R. E. Olson, 9571
9042	M. R. Birnbaum, 8742
9042	M. L. Chiesa, 8741
9042	L. E. Voelker, 8742
9042	J. J. Dike, 8743

9042	M. Horstemeyer, 8743
0899	Technical Library, 4916 (5)
0619	Review and Approval Desk, 12690 (2) for DOE/OSTI
9018	Central Technical Files, 8940-2